AGU ADVANCING EARTH AND SPACE SCIENCES

JGR Oceans

RESEARCH ARTICLE
10.1029/2023JC020374

Evaluation of the Water Mass Composition in the Sea of Okhotsk and Its Long-Term Change Using an Advanced Mapping Technique

Vigan Mensah[1], **Kay I. Ohshima**[1,2], **Robert Drucker**[3], **and Stephen Riser**[3]

[1]Institute of Low Temperature Science, Hokkaido University, Sapporo, Japan, [2]Arctic Research Center, Hokkaido University, Sapporo, Japan, [3]School of Oceanography, University of Washington, Seattle, WA, USA

Key Points:

- The composition of the Okhotsk Sea Intermediate Water (OSIW) is reevaluated using an updated data set and a new mapping technique
- OSIW properties have changed in the long-term (≥50 years) scale, with a decrease (increase) in the amount of heavy (light) Dense Shelf Water
- This suggests that the North Pacific intermediate overturning is weakening, which could affect the ocean's biological productivity

Supporting Information:

Supporting Information may be found in the online version of this article.

Correspondence to:

V. Mensah,
vmensah@lowtem.hokudai.ac.jp

Citation:

Mensah, V., Ohshima, K. I., Drucker, R., & Riser, S. (2024). Evaluation of the water mass composition in the Sea of Okhotsk and its long-term change using an advanced mapping technique. *Journal of Geophysical Research: Oceans*, *129*, e2023JC020374. https://doi.org/10.1029/2023JC020374

Received 15 AUG 2023
Accepted 18 JUN 2024

Author Contributions:

Conceptualization: Vigan Mensah, Kay I. Ohshima
Formal analysis: Vigan Mensah
Funding acquisition: Kay I. Ohshima
Investigation: Vigan Mensah
Methodology: Vigan Mensah, Robert Drucker
Project administration: Kay I. Ohshima
Resources: Stephen Riser
Supervision: Kay I. Ohshima
Validation: Vigan Mensah, Robert Drucker
Visualization: Vigan Mensah
Writing – original draft: Vigan Mensah
Writing – review & editing: Kay I. Ohshima, Stephen Riser

Abstract The Sea of Okhotsk is a marginal sea that plays a major role in the ventilation of the North Pacific, being the key location where Dense Shelf Water (DSW) forms at the surface and sinks to the intermediate layer. The Okhotsk Sea Intermediate Water (OSIW) is a key water mass because it includes large amounts of DSW, outflows to the North Pacific, and supplies the ocean with the micronutrient iron. OSIW has been warming over the past few decades, which is attributed to a decreasing trend in DSW production. The acquisition of numerous hydrographic data after 2000 in the Kuril Basin, especially dissolved oxygen from profiling floats, offers an opportunity to better quantify the water mass composition of OSIW, and the changes in OSIW properties and DSW volume. Here, we used all available hydrographic records and a mapping technique specially adapted to polar and sub-polar regions to revisit the Sea of Okhotsk water properties and document their long-term changes. Our analysis revealed that the volume of heavier DSW (potential density above 26.9 kg.m^{-3}) has decreased over the past three decades by 3,600 km^3, or 15% of the volume present before 1990. This decline is nearly entirely compensated for by an increase in lighter DSW. This shift toward lighter DSW is possibly a sign of the weakening of the intermediate overturning circulation starting in the Okhotsk Sea. Additionally, we found that dense Soya Current Water only accounts for about 1% of OSIW, against the 5% previously estimated.

Plain Language Summary The water of the Sea of Okhotsk is a mix of several water masses which includes the Dense Shelf Water (DSW), a water mass generated in winter via sea ice formation. When sea ice forms, the surface water salinity and density increase, and the cold DSW is generated as the surface water sinks to the bottom of the continental shelf while micronutrients, especially iron, are also incorporated. DSW mixes with other water masses and becomes the Okhotsk Sea Intermediate Water (OSIW) before being exported to the North Pacific where it plays an important role for both the climate and the biological productivity. In this study, we used all the temperature, salinity, and dissolved oxygen data acquired since 1930 to evaluate how global warming may have affected the composition of OSIW. We found that, over the past century, the amount of denser DSW has strongly decreased whereas that of lighter DSW has increased, which is consistent with the decline in sea ice production in the Sea of Okhotsk. This also suggests that the ventilation of the Sea of Okhotsk and the circulation of the intermediate layer of the North Pacific is weakening, which could indirectly affect the ocean's biological productivity.

1. Introduction

The Okhotsk Sea intermediate water (OSIW) is a cold, oxygen-rich, and iron-rich intermediate water mass that flows out to the North Pacific via the Kuril Straits (Itoh et al., 2003; Nishioka et al., 2007; Ohshima et al., 2010). There, by mixing with warmer, oxygen-rich, and nutrient-rich water from the subarctic Pacific, it forms Oyashio water and subsequently North Pacific Intermediate Water (Kono & Kawasaki, 1997; Riser, 1996; Talley, 1993; Yasuda, 1997). Because both iron and nutrients such as nitrate and phosphate are crucial to phytoplankton growth, mixing of the subarctic waters with OSIW plays a crucial role in making the mixed water region of the northwest Pacific one of the major biological productivity hotspots in the world's ocean (Nishioka et al., 2020). As such, the Sea of Okhotsk is a marginal sea of great importance to the North Pacific Ocean.

OSIW also plays a major role in the ocean's circulation and climate as the Sea of Okhotsk is a key location for the ventilation of the North Pacific. A large amount of sea ice forms in the coastal polynyas of the Sea of Okhotsk, particularly the northwestern shelf and the Sakhalin polynyas (Gladyshev et al., 2000; Martin et al., 1998; Nakata & Ohshima, 2022; Nihashi et al., 2009), and through this process, the surface water cools to the freezing point while salinity increases due to brine rejection. This cooling and salinification lead to a strong increase in the surface water density and convection, thus forming Dense Shelf Water (DSW). This water sinks to the intermediate layer due to its high density, which constitutes a starting point for the North Pacific overturning (Shcherbina et al., 2003). DSW flows to the Sea of Okhotsk's Kuril Basin and mixes with other waters along its path to become OSIW, which inherits DSW's cold, oxygen-rich, and iron-rich properties. The residence time of OSIW in the Kuril Basin of the Okhotsk Sea is about 1 year (Ohshima et al., 2010), following which OSIW flows out to the North Pacific via the Kuril Straits. Hereafter, the series of processes including the DSW generation and sinking in the Sea of Okhotsk, intermediate water formation, and its transport from the Sea of Okhotsk to the North Pacific, will be referred to as the North Pacific intermediate overturning. Thus, the fraction of DSW within OSIW is a major factor influencing the intermediate overturning and water properties of the North Pacific.

The water masses formation, composition, and transport in and out of the Sea of Okhotsk were extensively described by Itoh et al. (2003). OSIW results from the mixing of DSW with the warmer western subarctic water (WSAW) and dense Soya Current Water (dSCW). The WSAW originates from the Bering Sea and is transported via the East Kamchatka Current toward the Kuril Islands (Andreev & Shevchenko, 2008; Ohtani et al., 1972; Rogachev, 2000; Stabeno et al., 1994), where a part of its flow is diverted to the Sea of Okhotsk (Shu et al., 2021). The dSCW—also known as Forerunner of Soya Current Water (Itoh et al., 2003; Takizawa, 1982; Watanabe & Wakatsuchi, 1998)—is generated in spring in the Japan Sea due to the integrated cooling of salty sub-tropical waters originating from the Kuroshio water (Chiba et al., 2021). Itoh et al. (2003) estimated OSIW at the 26.8 σ_θ density level as a mix of 44% DSW, 51% WSAW, and 5% dSCW. There was, however, a limited number of dissolved oxygen (DO) profiles in the Kuril Basin before 2000, and the interpolation of sparse data may have reduced the accuracy of the previous water mass composition analyses, especially regarding the fraction of dSCW, which is distinguishable through its high DO.

The interannual to bi-decadal variability of OSIW properties is related to changes in the intensity of the North Pacific subarctic gyre, sea ice production, and the 18.6-year cycle of the diurnal tide. The Aleutian Low spins up the subarctic gyre and a relationship exists between the strength of the Aleutian Low and the influx of WSAW to the Okhotsk Sea (Andreev & Baturina, 2006; Prants et al., 2015). Ohshima et al. (2010) explained the variability of the WSAW inflow based on the island rule (Godfrey, 1989), by the Sverdrup transport over the North Pacific, whereas Uehara et al. (2014) and Matsuda et al. (2015) suggested that interannual variations in the properties of DSW or/and OSIW are caused by the advection of surface salinity anomalies across the subarctic gyre. Variability in the sea ice production could also affect OSIW properties as Kashiwase et al. (2014) found a significant relationship between sea ice production in the northern Sea of Okhotsk and OSIW temperature. Besides the interannual variabilities, periodic bi-decadal variations of the OSIW or Oyashio water properties have been observed in several studies (Andreev & Baturina, 2006; Itoh, 2007; Mensah & Ohshima, 2021; Ono et al., 2001; Osafune & Yasuda, 2006) and attributed to the 18.6-year cycle of the diurnal tide.

In the long term (from the bi-decadal to the century-scale), the North Pacific has been warming and this has been linked to a warming trend of OSIW (Nakanowatari et al., 2007; Ono et al., 2001). Several works proposed that the multi-decadal decrease in the Okhotsk Sea ice production (Kashiwase et al., 2014) is responsible for the weakening of the North Pacific intermediate overturning (Itoh, 2007; Mensah & Ohshima, 2021; Ohshima et al., 2014). These studies suggest that the decline in sea ice production led to smaller volumes of DSW being produced, resulting in warming, an increase in salinity, and a decrease in DO of OSIW. Other studies suggest that the strengthening of the Aleutian Low could explain the changes in OSIW properties via the increase in WSAW flux to the Sea of Okhotsk, and the warming, salinification, and loss of DO of WSAW (Andreev & Baturina, 2006; Andreev & Watanabe, 2002). Thus, changes in the relative volume of WSAW and DSW within the Kuril Basin should be examined to clarify the processes responsible for OSIW long-term variability.

Such evaluations are made possible by the acquisition of numerous hydrographic data since the early 2000s—especially DO profiles—and progress in the mapping of data in sub-polar and polar regions. Several thousand profiles of temperature, salinity, and dissolved oxygen have indeed been obtained in the last two decades in the Kuril basin by profiling floats (Kishi et al., 2021; Mensah et al., 2019; Ohshima et al., 2010). Besides, Mensah and Ohshima (2023) have proposed a new mapping methodology adapted to the sub-polar and polar regions, which reduces the mapping errors and refines the resolution of frontal structures, such as the front which separates dSCW from the other waters in the Sea of Okhotsk.

In this paper, we used all conductivity-temperature-depth (CTD) and dissolved oxygen data available in the southern Sea of Okhotsk between 1930 and 2022 to produce climatologies and (a) reevaluate the fraction of dSCW within OSIW, and (b) quantify the long-term changes in the volume of DSW in the Kuril Basin. In the process of evaluating these quantities, the respective fractions of DSW, WSAW, and dSCW will be estimated before and after 1990. The hydrographic data set, mapping methodology, and the method used to estimate the water masses fractions will be briefly described in Section 2. We will then introduce the results of water mass fractions in Section 3, and DSW volume and its changes in Section 4. The results reveal a lesser amount of dSCW within OSIW than previously thought and significant lightening of the DSW. Section 5 will be dedicated to a discussion on the significance of these results for the Sea of Okhotsk and the North Pacific, and how these results relate to the weakening of the North Pacific intermediate overturning. Section 6 will present a summary and conclusions of this study.

2. Data and Methods

2.1. Hydrographic Data

The data set's main sources of data are the World Ocean Database 2018 (WOD18, Boyer et al., 2018) and about 2,500 profiles from profiling floats deployed as part of a Hokkaido University-University of Washington joint project (archived in the Arctic Data archive System of the Japanese National Institute of Polar Science, Mensah et al., 2024) as well as a Japan, Russia, and USA joint study. The WOD18 data set includes CTD data as early as 1933 and the profiling float data were acquired between 2000 and 2018. These data sources are supplemented by biologging data from 7 seal and sea lions deployed in 2015 (Nakanowatari et al., 2017) and CTD data acquired during various cruises by the Russian R/V Khromov (1998, 1999, 2000, 2006, 2007), the Japanese R/V Shinsei Maru (2021, 2022), and the rented fishing vessel Seikou Maru (2022). Additional data acquired off the Hokkaido coast between 2006 and 2022 were provided by the Wakkanai Fisheries Research Institute. In total, 10,975 potential temperature and salinity profiles are available in the southern Sea of Okhotsk (Figure 1), including 5698 profiles acquired until 1990, and 5586 profiles from 1990 onward. The number of dissolved oxygen (DO) profiles is 3307, including 1763 profiles and 1579 acquired until 1990, and from 1990, respectively (the data of 1990 was included for both climatologies). The DO data were calibrated following Drucker and Riser (2016) and details of the calibration are provided in Text S1 of the Supporting Information S1. The distribution of all available data at the 26.7 potential density (σ_θ) level before and after 1990 is presented in Figures 1a and 1b.

These hydrographic data were used to produce annual and seasonal (January–April, May–August, September–December) climatologies for the periods 1930–2022, 1930–1990, and 1990–2022, using the shrinking stretching constraint integrated (SSCI) mapping scheme of Mensah and Ohshima (2023). This allows us to estimate long-term trend changes affecting the Sea of Okhotsk as well as changes in the volume of DSW in the Kuril Basin.

2.2. Mapping Methodology

In polar and subpolar regions, the dominant constraint on the weakly stratified water column is the conservation of potential vorticity, which can be expressed in the mean state as $P = f/H$, where H is the bottom depth and f is the Coriolis parameter. The SSCI mapping scheme uses this principle by including a water column shrinking and stretching constraint in addition to a distance constraint to map observations into a gridded domain as follows:

$$W(r, \Delta h) = \exp\left[-\left(\frac{r}{L_r}\right)^2 - \left(\frac{\Phi}{L_\Phi}\right)^2\right], \tag{1}$$

where r represents the distance between the grid point and the observation and $\Phi = \Delta h/h$ is the ratio of stretching at the observation point over that at the grid point (Δh being the depth difference between the bottom depth at the observation point and the bottom depth h at the grid point), and L_r and L_Φ are the decorrelation scales.

The various climatologies are produced on a 5 × 5 km resolution grid whose domain is shown in Figure 1b, at several σ_θ levels, that is, 26.7 σ_θ–27.3 σ_θ at an interval of 0.1 σ_θ. This vertical range covers the intermediate water layer, usually defined as 26.8–27.3 σ_θ (~200–800 m). We added the 26.7 σ_θ level since this layer represents the extreme limit reached by winter convection in the Sea of Okhotsk (Gladyshev et al., 2003), and, similar to denser layers, this level is less affected by seasonal variability than less dense layers.

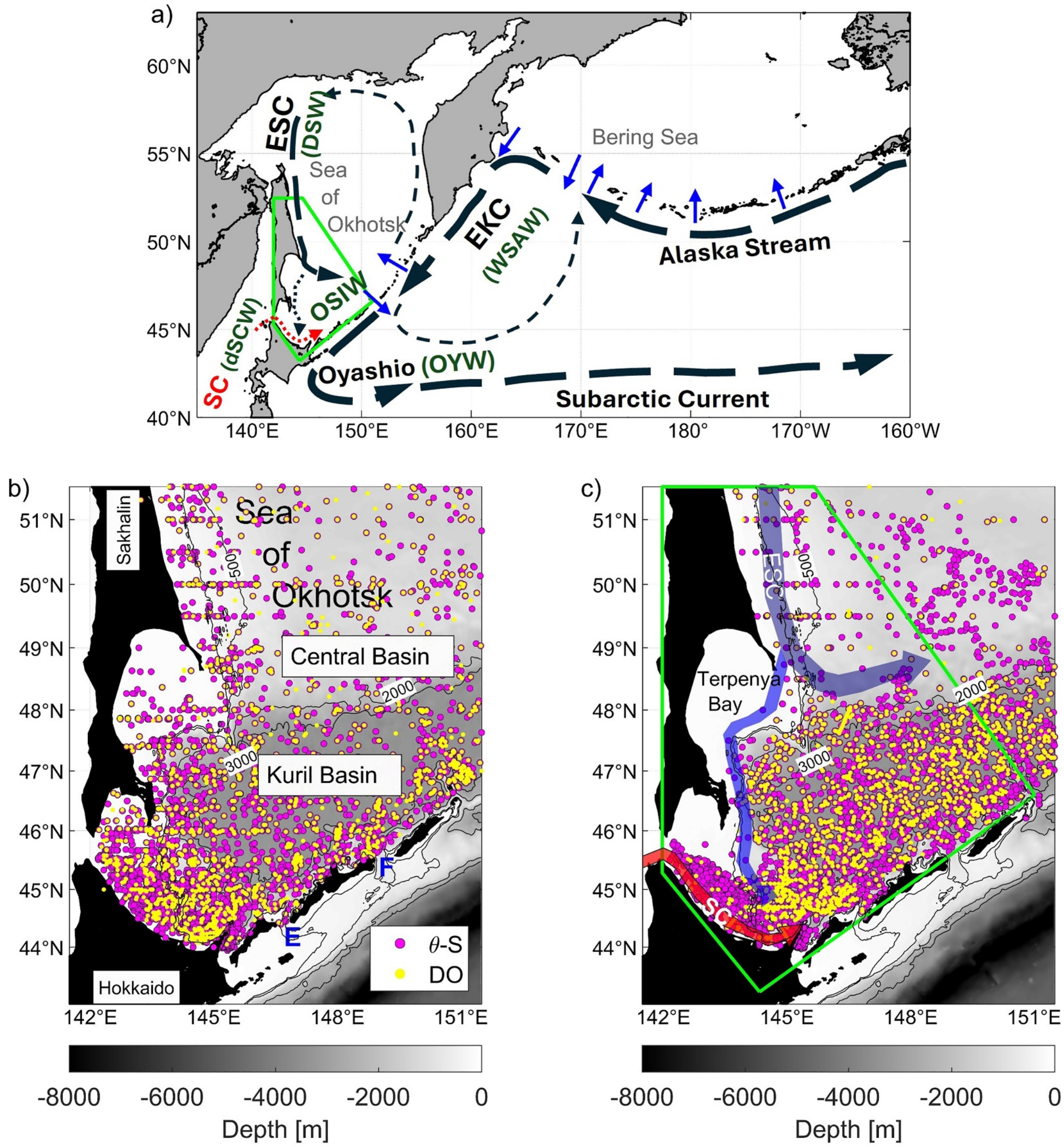

Figure 1. (a) Schematic view of the main currents in the subarctic gyre and the Sea of Okhotsk. ESC, SC, and EKC stand for the East Sakhalin Current, the Soya Warm Current, and the East Kamchatka Current. The intermediate Water masses mentioned in this paper are written in dark green. The blue arrows indicate the locations where the water masses of the Bering and Okhotsk Sea are exchanged with those of the subarctic gyre. The North Pacific Intermediate Water (NPIW) is formed from OYW south of the subarctic current. (b and c) Bathymetry (gray shading) and distribution of temperature-salinity (pink dots) and dissolved oxygen (yellow dots) for (b) the period 1930–1990, and (c) the period 1990–2022. In (b), the letters E and F stand for the Ekaterina Strait, and Friza Strait, respectively. These straits will be referred to hereafter as the Kuril Straits. In (c), the red arrow represents the pathway of the SC, the purple arrow that of the ESC, and the blue arrow the coastal branch of the ESC. The green boxes in (a) and (c) represent the study domain over which data were mapped.

Mensah and Ohshima (2023), taking the Sea of Okhotsk as an example, demonstrated that the SSCI method yielded significantly lower error than several other mapping methodologies in regions having a broad and shallow shelf connected to the deep basin by a sharp continental slope, which is a topographic setting typical of polar and subpolar marginal seas. Thus, to illustrate the significance of using the SSCI mapping in the context of our study, we compare the yearly 1930–2022 climatology of dissolved oxygen obtained through this method and that obtained with the iso-directional weighted mean mapping method used by Itoh et al. (2003). The decorrelation scales in the Sea of Okhotsk are $L_r = 97$ km and $L_\Phi = 0.56$ for the SSCI mapping (Mensah & Ohshima, 2023), and $L_r = 75$ km for the iso-directional mapping (Itoh et al., 2003; Ohshima et al., 2014).

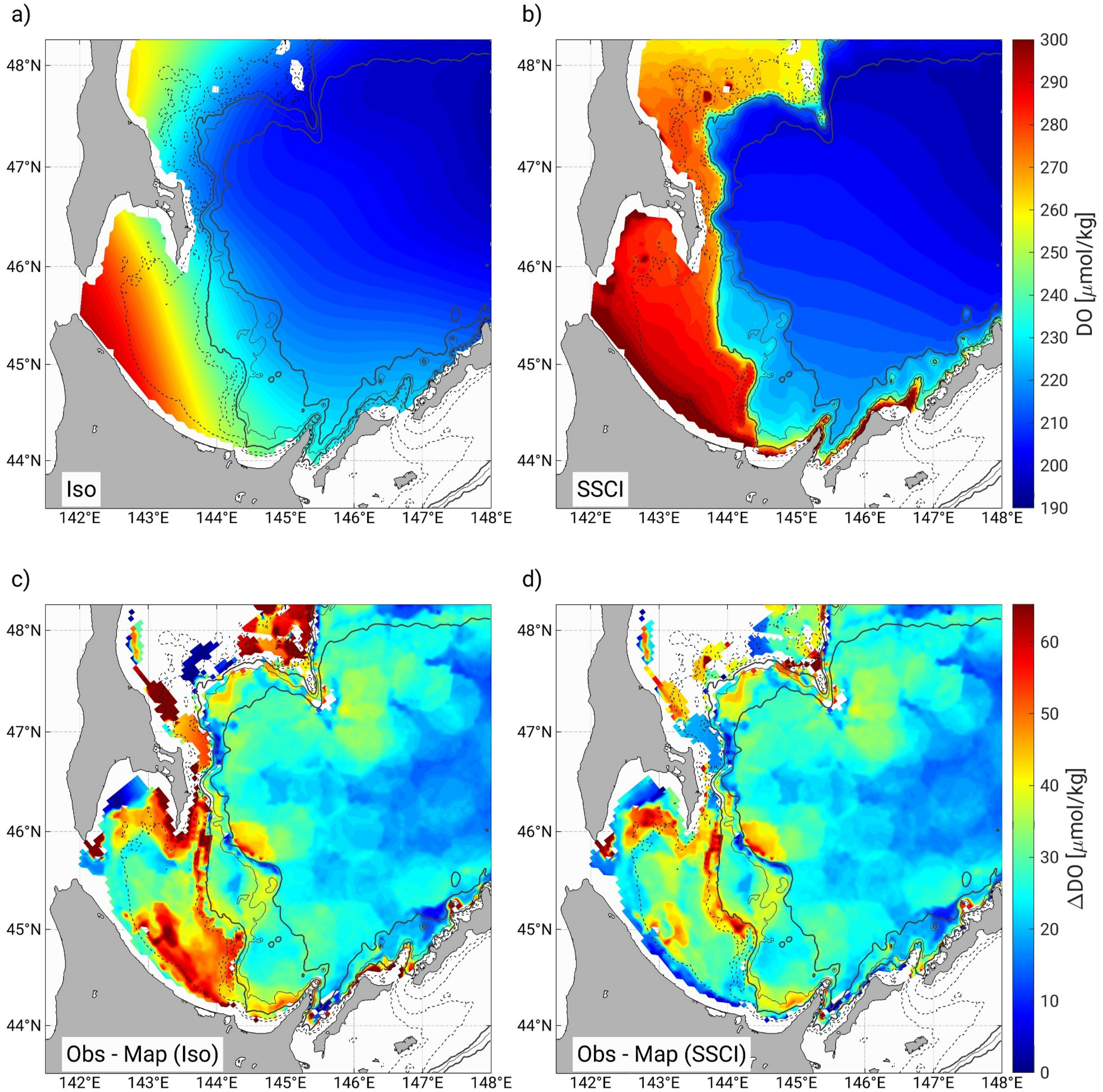

Figure 2. Mapped distribution of all dissolved oxygen data (1930–2022) in the southern Sea of Okhotsk at 26.8 σ_θ obtained with (a) iso-directional weighted mean with $L_r = 75$ km, (b) SSCI mapping scheme with $L_r = 97$ km and $L_\Phi = 0.56$. Panels (c, d) represent the root mean square difference (error) between observed and mapped data with each of the respective methodologies.

Figures 2a and 2b respectively show the SSCI and iso-directional climatologies at 26.8 σ_θ, and Figures 2c and 2d displays the root mean square difference estimated between observed and mapped values within one decorrelation scale L_r and L_Φ of each grid point, for the two methods. The SSCI method results in better-defined properties on the shallow shelf and frontal regions, whereas the iso-directional mapping yields a considerably smoother climatology (Figures 2a and 2b). This smooth climatology produces a particularly large error on the shelf regions (Figure 2c). In effect, this smoothing artificially spreads the dSCW properties far away from the Hokkaido coast and even into the Kuril Basin. Due to this problem, the fraction of dSCW in the Kuril Basin and OSIW was presumed to be relatively high in previous studies (Itoh et al., 2003; Watanabe & Wakatsuchi, 1998). In contrast, the SSCI mapping yields a smaller error in our study domain (Figure 2d) and the high DO content all along the Hokkaido coast and the southwestern Kuril Islands is more consistent with the observations (e.g., Chiba

10.1029/2023JC020374

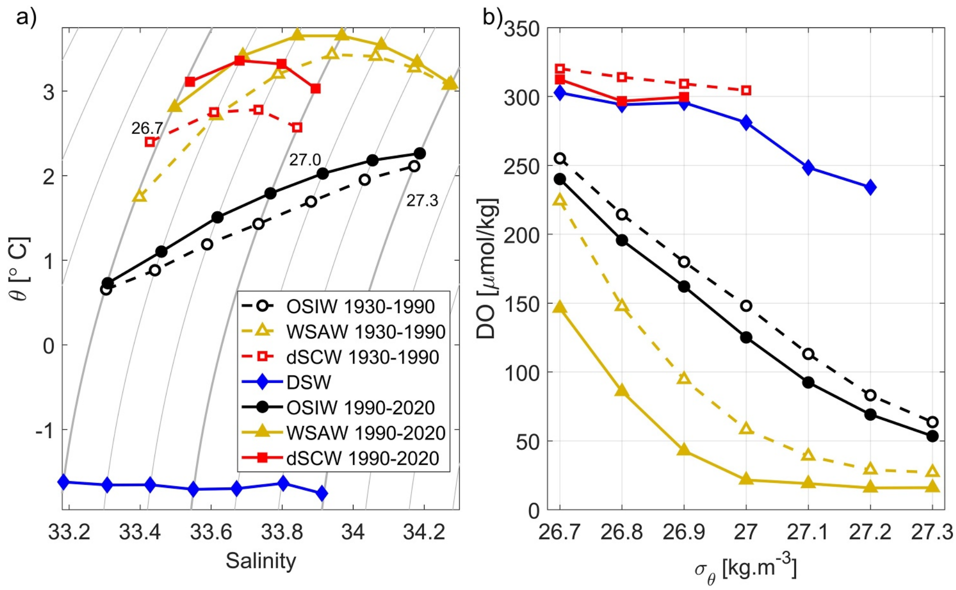

Figure 3. (a) *θ*-*S* diagram of OSIW and its three source waters for the periods 1930–1990 and 1990–2022. (b) Dissolved oxygen properties of the same water masses as a function of potential density.

et al., 2021). Such results motivated us to re-estimate the fraction of dSCW in OSIW, using the method delineated in the following section.

2.3. Water Masses Definition

The properties of WSAW, dSCW, and DSW have been defined by Itoh et al. (2003) but may have changed significantly between the periods 1930–1990 and 1990–2022. Such is the case, for example, for WSAW (Andreev & Baturina, 2006; Mensah & Ohshima, 2021). We will therefore update the definitions of these water masses for each of the two periods studied in this paper and their combined period (1930–2022). OSIW is defined here as all the water in the Kuril Basin where the depth is greater than 2,000 m.

The properties of dSCW are obtained by averaging climatological data within 45 km of the coast of Hokkaido between April and June, similar to the definition of Itoh et al. (2003). An April–June climatology was produced specifically for this purpose. These 3 months were chosen because they correspond to the period when the highest amount of dSCW exists along the Hokkaido coast (Itoh et al., 2003; Ohshima et al., 2017). The dSCW properties were estimated in this way for the period 1930–1990 and 1990–2020 (Figure 3). The values for the period 1930–2020 were obtained by averaging those of each of the pre- and post-1990 periods.

WSAW properties are obtained from a November to March climatology generated from WOD18 data using the same methodology (Section 2.2) since the inflow of WSAW into the Sea of Okhotsk is relatively strong between November and March (Ohshima et al., 2010; Prants et al., 2015). The definition region for this water mass is north of 49°N, west of 165°E, and within the 1,000 m and 3,000 m isobaths. This was done because the water entering the Sea of Okhotsk belongs to the East Kamchatka Current, a western boundary current that typically does not flow over the shallow Kamchatka shelf (e.g., Andreev & Pipko, 2022; Shu et al., 2021; Stabeno et al., 1994). Similarly to dSCW, the 1930–2022 properties of WSAW (Table 1) were obtained by averaging those of the pre- and post-1990 periods (Figure 3).

The definition of DSW was updated by using the monthly Okhotsk Sea climatology of Uehara et al. (2012), defining DSW at each density level as the water colder than −1.5°C between 54°N and 60°N. The climatology of Uehara et al. (2012) is made from numerous Russian data not publicly available, making it a unique source of information. Using this climatology, DSW was detected up to 27.3 σ_θ, that is, denser than the maximum density of 27.0 σ_θ previously reported (Gladyshev et al., 2003; Shcherbina et al., 2003). The same values were used for all three time periods, which is reasonable since DSW is generated via sea ice formation and its temperature is thus always close to the freezing point.

Table 1
θ, Salinity, and Dissolved Oxygen Properties of OSIW and Its Three Source Waters (WSAW, dSCW, DSW) and Its 90% Confidence Interval for the Climatological Period 1930–2022

		θ (°C)	Salinity	DO (μmol/kg)
WSAW	26.7 σ_θ	2.28 ± 0.24	33.447 ± 0.023	185 ± 21
	26.8 σ_θ	3.06 ± 0.15	33.652 ± 0.016	117 ± 18
	26.9 σ_θ	3.43 ± 0.09	33.816 ± 0.011	69 ± 13
	27.0 σ_θ	3.54 ± 0.04	33.954 ± 0.006	40 ± 8
	27.1 σ_θ	3.48 ± 0.03	34.071 ± 0.004	29 ± 6
	27.2 σ_θ	3.31 ± 0.03	34.176 ± 0.004	22 ± 4
	27.3 σ_θ	3.08 ± 0.03	34.273 ± 0.005	22 ± 4
dSCW	26.7 σ_θ	2.76 ± 0.29	33.484 ± 0.034	316 ± 13
	26.8 σ_θ	3.06 ± 0.24	33.644 ± 0.024	305 ± 13
	26.9 σ_θ	3.05 ± 0.18	33.766 ± 0.020	304 ± 9
	27.0 σ_θ	2.80 ± 0.19	33.868 ± 0.020	305 ± 17
DSW	26.7 σ_θ	−1.62 ± 0.01	33.184 ± 0.001	303 ± 2
	26.8 σ_θ	−1.66 ± 0.01	33.307 ± 0.001	294 ± 2
	26.9 σ_θ	−1.65 ± 0.01	33.428 ± 0.001	296 ± 3
	27.0 σ_θ	−1.71 ± 0.02	33.549 ± 0.001	281 ± 6
	27.1 σ_θ	−1.70 ± 0.04	33.671 ± 0.002	248 ± 12
	27.2 σ_θ	−1.63 ± 0.02	33.803 ± 0.002	234
	27.3 σ_θ	−1.76	33.912	–
OSIW	26.7 σ_θ	0.68 ± 0.09	33.306 ± 0.006	245 ± 5
	26.8 σ_θ	1.00 ± 0.06	33.452 ± 0.005	202 ± 5
	26.9 σ_θ	1.38 ± 0.05	33.606 ± 0.004	168 ± 5
	27.0 σ_θ	1.66 ± 0.04	33.755 ± 0.004	133 ± 4
	27.1 σ_θ	1.92 ± 0.04	33.904 ± 0.004	99 ± 4
	27.2 σ_θ	2.11 ± 0.02	34.048 ± 0.002	73 ± 3
	27.3 σ_θ	2.21 ± 0.02	34.183 ± 0.002	57 ± 2

Note. The confidence interval was estimated from the standard error (RMS difference between raw data and mapped values, divided by the squared root of the raw data number) averaged within the water masses definition areas. The dSCW and DSW properties were estimated from climatologies, and no confidence interval was provided for values obtained from only one grid point.

The θ, salinity, and dissolved oxygen properties of each water mass for the climatological period of 1930–2022 are listed in Table 1, and those for the periods 1930–1990 and 1990–2022 are shown in Tables S1 and S2 of the Supporting Information S1 and Figure 3. As shown in the table, dSCW is the warmest, saltiest, and most DO-rich water, WSAW has the lowest DO, and DSW is the coldest and freshest water mass. All the estimates related to climatological differences between the pre- and the post-1990 climatologies (Sections 4 and 5) were obtained by using the water mass properties for the respective periods (Figure 3, Tables S1 and S2 in Supporting Information S1).

2.4. Estimation of Water Mass Fractions

The fractions of dSCW (F_{SCW}), DSW (F_{DSW}) and WSAW (F_{WSAW}) were calculated at each grid point via a least square method including θ, DO, and salinity:

$$\Sigma = \epsilon_\theta^2 + w_{\mathrm{DO}} \cdot \epsilon_{\mathrm{DO}}^2 + w_S \cdot \epsilon_S^2 \tag{2a}$$

where Σ is the sum of the squared errors in potential temperature ϵ_θ, salinity ϵ_S, and dissolved oxygen ϵ_{DO}, weighted by their respective coefficient w_{DO} and w_S:

$$\epsilon_\theta = (\theta_{\mathrm{SCW}} \cdot F_{\mathrm{SCW}} + \theta_{\mathrm{WSAW}} \cdot F_{\mathrm{WSAW}} + \theta_{\mathrm{DSW}} \cdot F_{\mathrm{DSW}}) - \theta_m \tag{2b}$$

$$\epsilon_{\mathrm{DO}} = (\mathrm{DO}_{\mathrm{SCW}} \cdot F_{\mathrm{SCW}} + \mathrm{DO}_{\mathrm{WSAW}} \cdot F_{\mathrm{WSAW}} + \mathrm{DO}_{\mathrm{DSW}} \cdot F_{\mathrm{DSW}}) - \mathrm{DO}_m \tag{2c}$$

$$\epsilon_S = (S_{\mathrm{SCW}} \cdot F_{\mathrm{SCW}} + S_{\mathrm{WSAW}} \cdot F_{\mathrm{WSAW}} + S_{\mathrm{DSW}} \cdot F_{\mathrm{DSW}}) - S_m \tag{2d}$$

$$F_{\mathrm{SCW}} + F_{\mathrm{WSAW}} + F_{\mathrm{DSW}} = 1 \tag{2e}$$

Here, θ_m, DO_m, and S_m are the gridded values of potential temperature, DO, and salinity. The weights w_{DO} and w_S are calculated as follows:

$$w_{\mathrm{DO}} = s_\theta^2 / s_{\mathrm{DO}}^2 \tag{2f}$$

$$w_s = s_\theta^2 / s_s^2 \tag{2g}$$

where s_θ^2, s_{DO}^2, and s_s^2 are the variances of all the raw potential temperatures, dissolved oxygen, and salinity within one decorrelation scale $L_r = 97$ km and $L_\Phi = 0.56$ of each grid point. The values of F_{SCW}, F_{DSW}, and F_{WSAW} are the ones that minimize the quantity Σ. The fraction of dSCW is determined at all grid points except on the Sakhalin shelf, where the value is set to 0.

To evaluate the validity of our water masses fraction evaluation, we calculated synthetic values of θ, salinity, and DO at all grid points in our study domain based on the respective fractions of dSCW, DSW, and WSAW and the properties of these source water masses (Table 1). Details of the validation results are delineated in Text S2 of the Supporting Information S1. The 90% confidence levels shown in the figures and tables were estimated based on Mensah and Ohshima (2021) and represent the sum of the mapping error and the error related to the properties' spatial variability in the water mass definition regions.

3. Water Masses Distribution and Fractions

3.1. dSCW

The distribution of θ and DO, and dSCW fraction throughout the study domain at the 26.8 σ_θ and 27.0 σ_θ layers are displayed in Figures 4 and 5, respectively, while the averaged dSCW fraction in OSIW at all density levels between 26.7 and 27. 0 σ_θ are listed in Table 2. On the broad shelf off Hokkaido, the dSCW and DSW-influenced

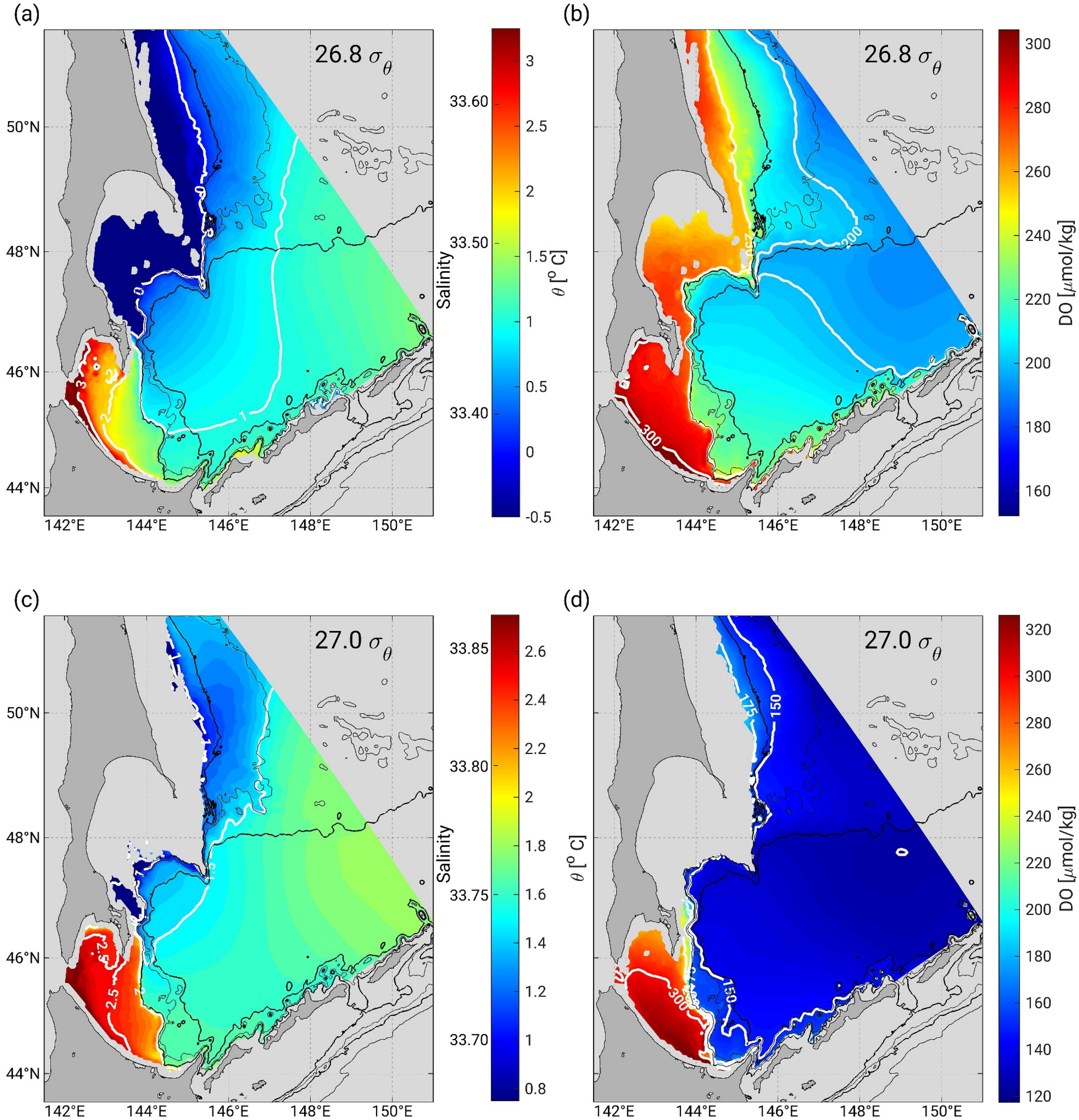

Figure 4. Mapped distribution of θ (a) and dissolved oxygen (b) at 26.8 σ_θ and (c, d) at 27.0 σ_θ for the period 1930–2022. On (a) and (c) the equivalent salinity values are indicated on the color bar.

waters are separated by a sharp front aligned with the 500 m isobath, also inferred from both the θ (Figures 4a and 4c) and DO (Figures 4b and 4d) climatologies. As exemplified in Figure 2d, the mapping error is small on either side of the front, indicating that this sharp change in θ and DO is a good representation of the physical reality. Correspondingly, the dSCW fraction drops sharply from values greater than 0.5 to nearly 0 from the nearshore to the offshore side of the front (Figures 5a and 5d). East of 144°E, the shelf becomes considerably narrower and the dSCW fraction decreases progressively toward the northeast. At 26.8 σ_θ, fractions greater than 0.1 exist only on the southwest side of the Kuril Basin, and no significant amount of dSCW is present in the rest of the basin. The fraction of dSCW averaged in the Kuril Basin is only 0.011 in this layer (Table 2), whereas it reaches 0.149 in the shallow regions off the Kuril Islands. This pattern of very low dSCW fractions in the Kuril Basin and high

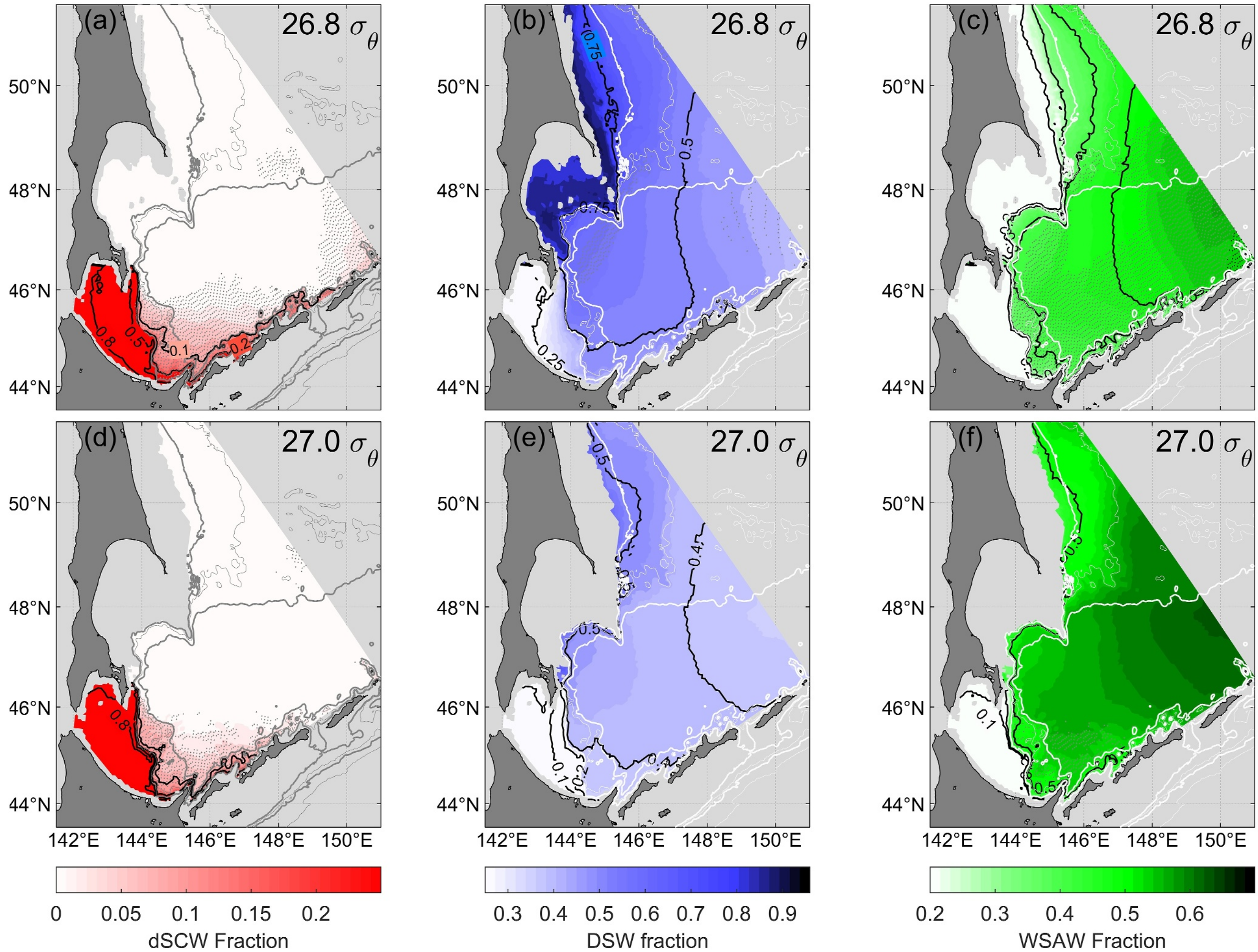

Figure 5. Mapped distribution of the fraction of dSCW (a, d), DSW (b, e), and WSAW (c, f) on the 26.8 σ_θ (a–c) and the 27.0 σ_θ layers (d–f) estimated from the mapped properties for the period 1930–2022. The areas with gray dots correspond to regions where the fractions uncertainty (at the 90% confidence level) ranges between 0.025 and 0.05. The uncertainty never exceeds 0.05.

fractions off the Kuril straits exists at every density layer (Table 2). Overall, the average fractions does not change with density, and the distribution of dSCW in the Kuril Basin at 27.0 σ_θ is not significantly different than that at 26.8 σ_θ (Table 2, Figure 5d).

The results of this analysis yield average dSCW fractions in OSIW ranging between 0.006 and 0.045 depending on the density layer (Table 2). These results suggest that most of dSCW does not enter the Kuril Basin and instead

Table 2
Fractions of WSAW, dSCW, and DSW in OSIW for the Climatological Period 1930–2022

σ_θ	WSAW	DSW	SCW	SCW (Kuril Straits)
26.7 σ_θ	0.482 (±0.069)	0.473 (±0.045)	0.045 (±0.047)	0.243 (±0.053)
26.8 σ_θ	0.492 (±0.032)	0.497 (±0.022)	0.011 (±0.022)	0.149 (±0.038)
26.9 σ_θ	0.537 (±0.018)	0.454 (±0.017)	0.008 (±0.015)	0.115 (±0.031)
27.0 σ_θ	0.588 (±0.013)	0.404 (±0.006)	0.006 (±0.011)	0.076 (±0.026)

Note. The last column on the right indicates the fraction of dSCW in regions with bottom depths shallower than 2,000 m off the Kuril Islands, in the Sea of Okhotsk. The numbers in brackets indicate the 90% confidence interval for each fraction, estimated following Mensah and Ohshima (2021).

follows the isobaths to exit the Sea of Okhotsk via the Kuril Straits. This would explain the high dSCW fractions found in the vicinity of the Kuril Islands (Table 2). The existence of high fractions at these locations is consistent with the distribution of dSCW estimated from raw data by Chiba et al. (2021). Lastly, the values estimated in this study are significantly smaller than the 0.05 dSCW fraction previously assumed to be part of OSIW (Itoh et al., 2003). We note that the uncertainty in dSCW fractions at 26.7 σ_θ and 26.8 σ_θ is relatively large (Table 2), which might be due to the uncertainty in dSCW and WSAW properties at these layers (Table 1).

3.2. DSW and WSAW

The distribution of the DSW fraction (Figures 5b and 5e) reflects well that of θ (Figures 4a–4c), that is, the DSW fraction increases with decreasing potential temperatures. On the shelf off Sakhalin Island at 26.8 σ_θ, the location of the 0°C isotherm (Figure 4a) matches that of the 0.75 DSW fraction, and the maximum fraction on this shelf is 0.90 near the southern tip of Sakhalin Island (Figure 5b). This suggests that there is little water mass transformation along the pathway of DSW from its formation region north of 54°N to the shelf of the southern Sea of Okhotsk.

At 26.8 σ_θ, the DSW fraction drops sharply beyond the 500 m isobath and then decreases eastward from the continental slope off Sakhalin toward the interior of the Kuril Basin. Still, the fraction remains higher than 0.5 west of 147°E (Figure 5b), and this relatively large DSW influence explains the low temperature and relatively high DO content in the northwestern part of the Kuril Basin (Figures 4a and 4b). Conversely, in the northeastern Kuril Basin where WSAW is dominant (Figure 5c), temperatures are higher and DO is lower. The distribution of WSAW mirrors that of DSW: the fraction decreases from the northeast of the Kuril Basin toward the southwest and drops close to the Sakhalin and Hokkaido shelves.

No water of density equal to or greater than 27.0 σ_θ exists over the Sakhalin shelf (Figures 5e and 5f), which is the most remarkable difference compared to the less dense levels (e.g., Figures 5b and 5c). This is also consistent with Gladyshev et al. (2003)'s suggestion that the densest waters formed on the northwestern shelf flow down and along the continental slope from their formation region to the Kuril Basin. These waters would then mix along their pathway with WSAW and older OSIW. The DSW fraction is notably lower at 27.0 σ_θ than at 26.8 σ_θ, decreasing from 0.45 to 0.35 from the western side to the eastern side of the Kuril Basin at 27.0 σ_θ (Figure 5e). As a result of these lower DSW concentrations, DO levels are considerably lower in the basin at 27.0 σ_θ (Figure 4d) than 26.8 σ_θ (Figure 4b).

4. Long-Term Changes in OSIW Properties and DSW Volume

4.1. Long-Term Variations of OSIW Temperature, Salinity, and Dissolved Oxygen

The summer climatologies of θ and DO for the periods before and after 1990 (Figure 6) highlight the nature of the long-term changes affecting the Sea of Okhotsk. We chose the summer climatologies since Mensah et al. (2019) demonstrated that the flow of DSW into the Kuril Basin is the most prominent between May and August.

Differences in properties are not homogeneous over the 26.7 σ_θ layer (Figures 6a and 6b). The temperature has increased in the Soya Warm Current region and in most regions north of 47°N. However, the temperature along the direct pathway of DSW—from the southern Sakhalin shelf to the southern Kuril Basin—has decreased, which suggests an intensification in the flow of DSW. The distribution of DO difference is also heterogeneous (Figure 6d), and as a result, the changes of properties averaged over the Kuril Basin are not significant (Figures 7a–7c) at the 26.7 σ_θ layer.

In contrast, a clear shift toward higher θ (Figures 6e–6g) and lower DO (Figure 6h) is visible at the 27.0 σ_θ layer. The temperature has risen throughout the study domain since 1990, with the largest changes occurring along the pathway of the dSCW, as well as the northern Kuril Basin and the Central Basin (Figures 6f and 6g). The decline in DO content is also largest in the latter two regions (Figure 6h). Consistent with the large variations seen in Figures 6e–6h, the θ and salinity averaged over the Kuril Basin have largely risen after 1990 while DO has decreased (Figures 7a–7c). These significant changes in OSIW properties affect all layers from 26.8 σ_θ to 27.2 σ_θ.

The volume census of θ in the Kuril Basin (Figure 8) suggests an increase in the volume of colder DSW within the Kuril Basin at 26.7 σ_θ. Indeed, the peak volumes have shifted toward colder temperatures after 1990 in this layer. In contrast, the census at all the other layers exhibits a shift of the distribution toward warmer temperatures after

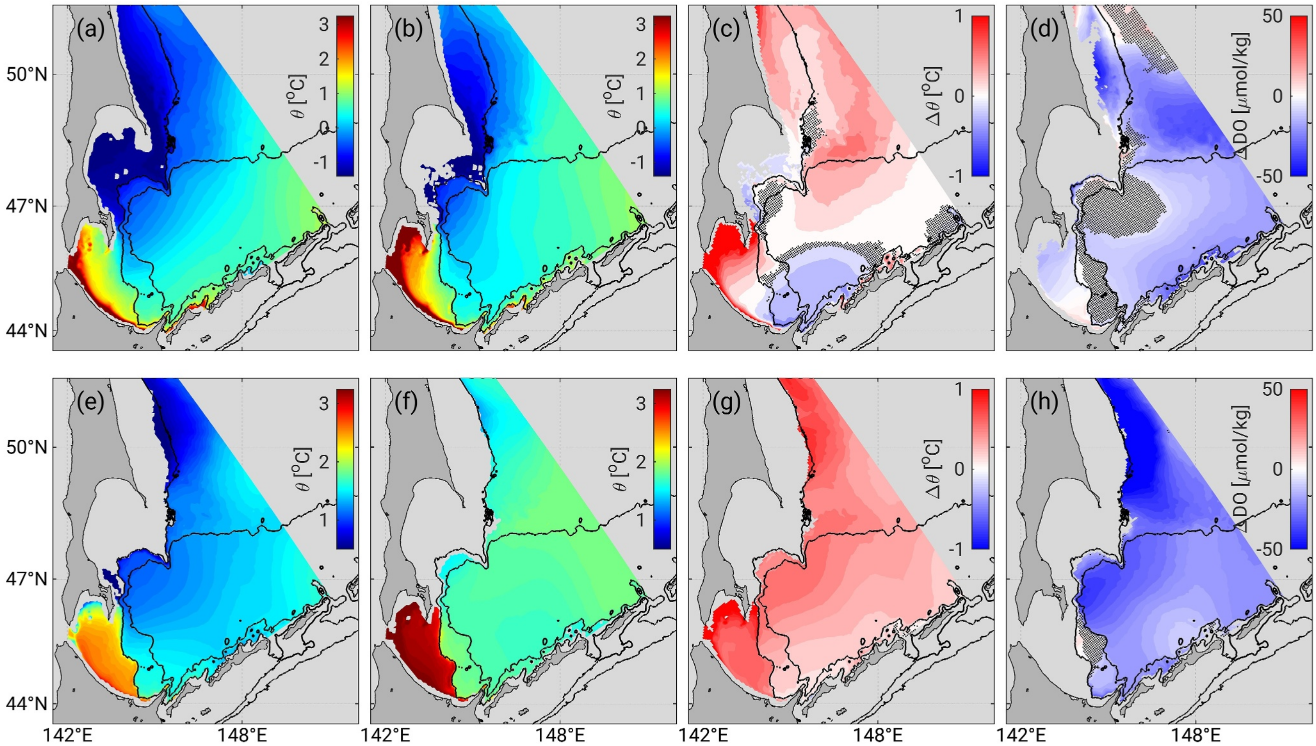

Figure 6. Mapped distribution of May–August (summer) θ at 26.7 σ_θ for the period (a) 1930–1990, (b) 1990–2022, (c) the θ, and (d) dissolved oxygen differences between the two periods (after minus before 1990). Panels (e–h) same as (a–d) but for the 27.0 σ_θ level. In (d) and (h), the areas with black dots represent regions where the difference in θ or DO is smaller than the 90% confidence level.

1990. Whether a decrease in the DSW fraction or the warmer WSAW after 1990 (Figure 3a) is responsible for the warm shift of the volume census is still unclear at this point.

Besides temperature, the volume occupied by each density layer in the Kuril Basin has also evolved (Figure 8h). The two uppermost density layers exhibit a large volume increase, with a nearly 30% change for the 26.7 σ_θ layer. This, combined with the relatively small changes in θ at 26.7 σ_θ and 26.8 σ_θ (Figures 8a and 8b), further supports

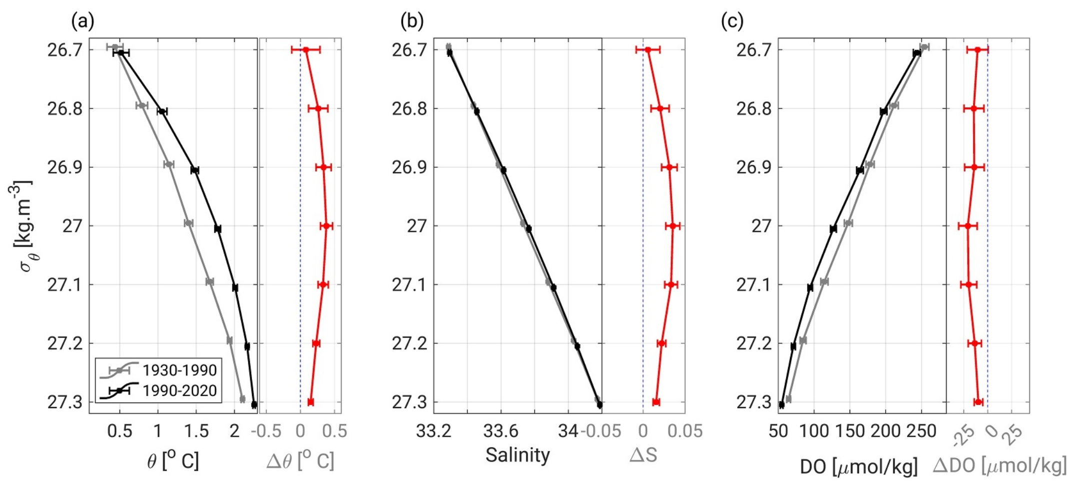

Figure 7. Vertical profiles of averaged summer climatological properties of OSIW for the period 1930–1990 (gray curve), and 1990–2020 (black curve) for (a) θ, (b) salinity, and (c) DO. The red curve on the right-hand panels of (a)–(c) indicates the difference between the two climatological periods. The OSIW properties were obtained by averaging all data at locations where the bottom depth exceeds 2,000 m. The error bars indicate the 90% confidence interval.

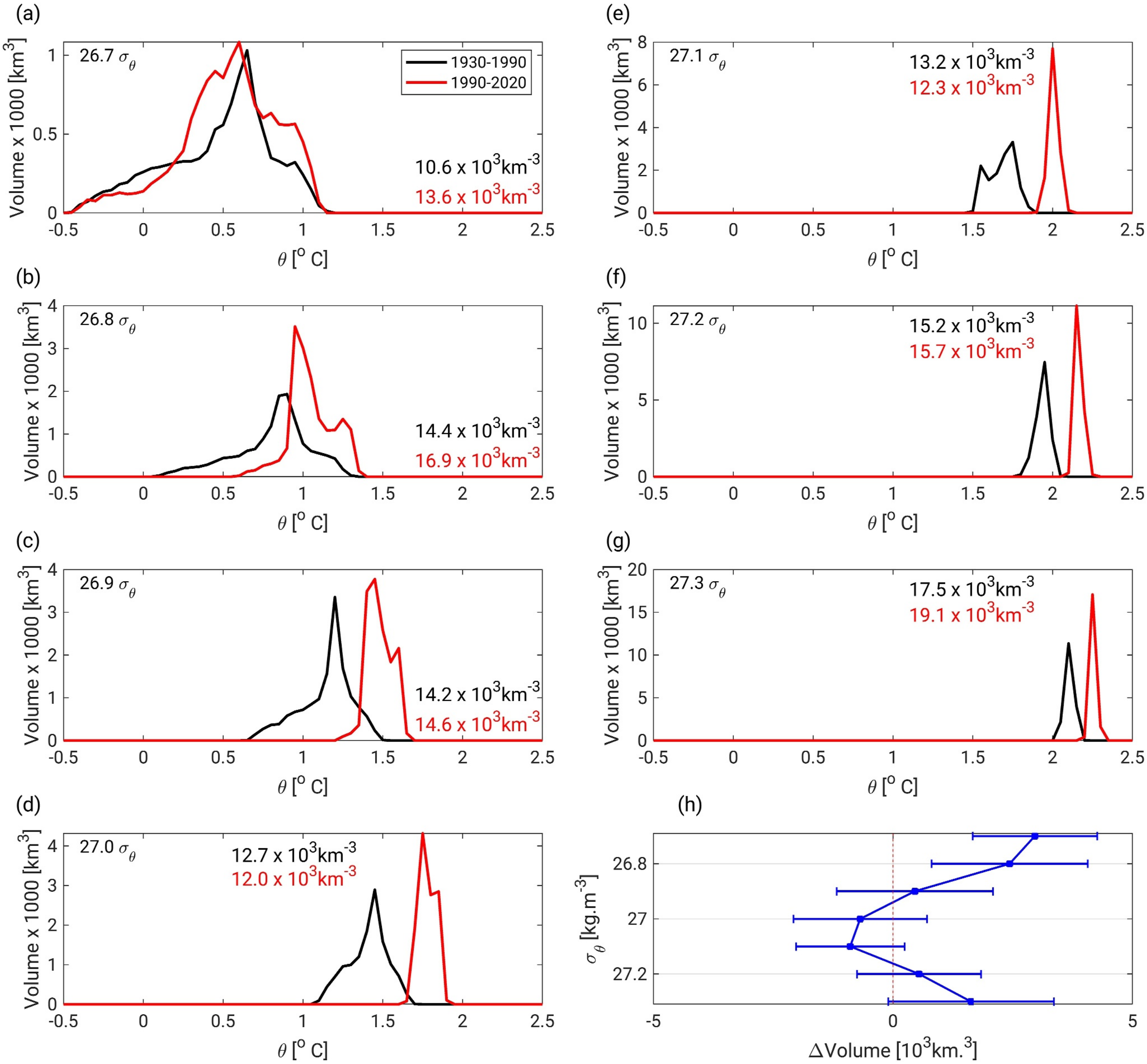

Figure 8. (a–g) Volume census of summer potential temperatures in the Kuril Basin (depth >2,000 m) for the period 1930–1990 (black curve), and 1990–2022 (red curve) for all density layers from 26.7 σ_θ to 27.3 σ_θ. The black and red numbers indicate the total volume of the isopycnal layer for their respective period. (h) Isopycnal layer volume thickness difference (1930–1990 minus 1990–2022). The error bars represent the 90% confidence interval. The isopycnal volume was estimated using climatologies of layer thickness following the methodology described in Section 2.2.

our hypothesis that DSW fraction has increased in these layers. On the other hand, the 27.0 σ_θ and 27.1 σ_θ layers have become thinner. Together with strong warming (>0.3°C, Figures 8c–8e), the thinning of these layers suggests a loss of DSW fraction. The combined changes in volume and temperature at the other layers are less conclusive since both the layer volume and θ have increased substantially after 1990. To further understand the extent to which changes in DSW fraction contribute to the long-term variations of OSIW properties, direct estimations of the DSW fraction for the 1930–1990 and 1990–2022 climatological periods are necessary.

4.2. DSW Fraction and Volume Changes

The distribution of DSW fractions for the two climatological periods and their differences reveal a clear contrast between the upper and lower intermediate waters (Figure 9). The 26.7 σ_θ layer is the only level where DSW

Journal of Geophysical Research: Oceans
10.1029/2023JC020374

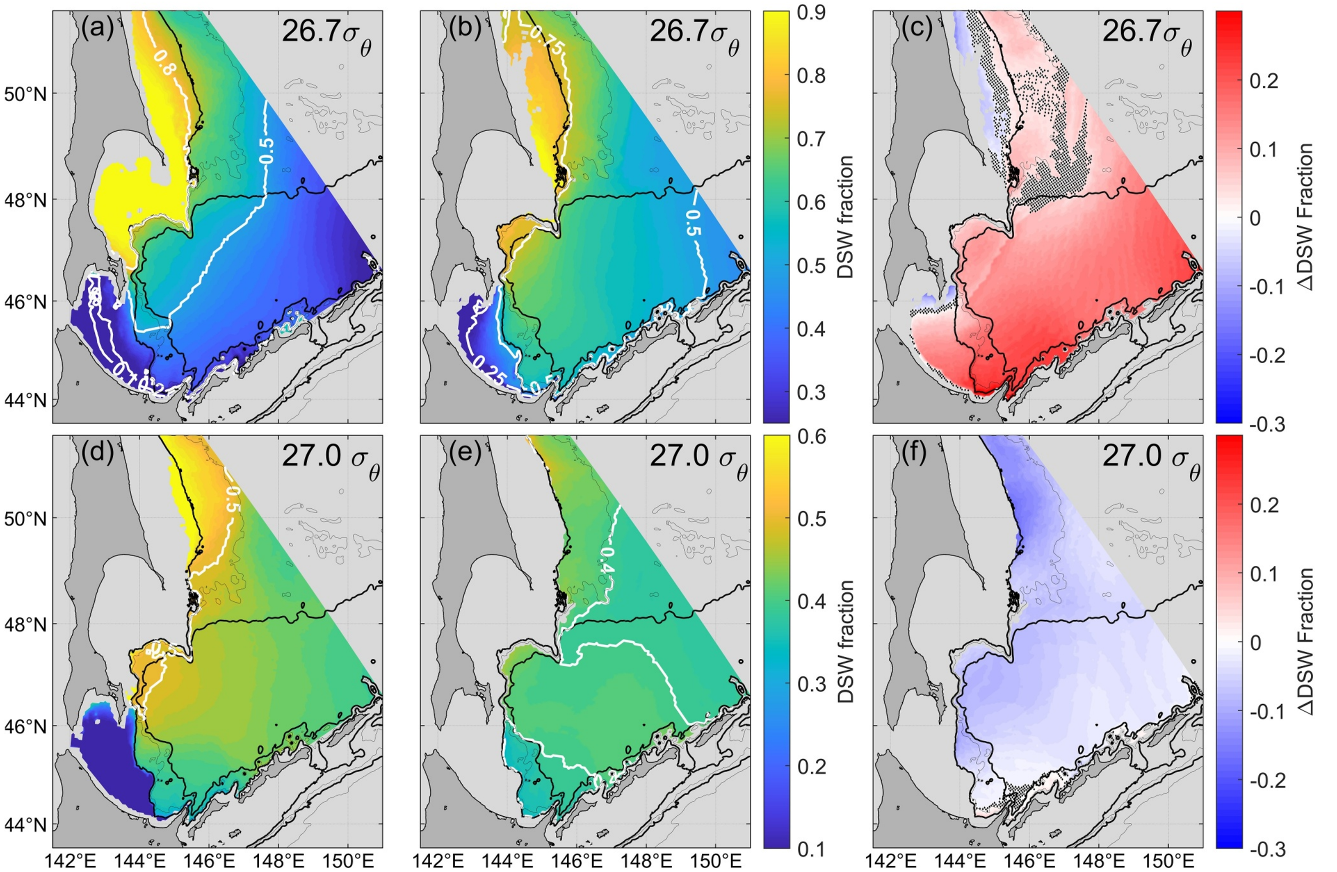

Figure 9. Mapped distribution of the summer DSW fraction at 26.7 σ_θ during the period (a) 1930–1990, (b) 1990–2022, and (c) their difference (1990–2022 minus 1930–1990). Panels (d–f) same as (a–c) but at 27.0 σ_θ. In (c) and (f), the areas with black dots represent regions where the fraction difference is smaller than the uncertainty (at the 90% confidence level).

fraction has significantly risen (Figures 9c and 10a), whereas all densities equal to or greater than 27.0 σ_θ exhibit significant drops in their DSW fraction (e.g., Figures 9d–9f and 10a). On average, the DSW fraction in the 27.0–27.3 σ_θ, has decreased by 15% since 1990, whereas no significant changes in DSW fraction occur at 26.8 σ_θ and 26.9 σ_θ. To illustrate that the changes affecting the DSW fraction and volume are effective throughout the year, and for statistical significance's sake, Figure 10 was made from yearly instead of summer data. Using summer data (not shown) yields similar results.

The complete picture of the long-term variability in DSW volume (Figure 10c) emerges when the changes in DSW fraction are combined with changes in isopycnal layer volume (Figures 8h and 10b). The uppermost two layers have become considerably thicker after 1990. This, combined with the gain in DSW fraction (Figure 10a), makes the DSW volume nearly twice higher after than before 1990 at 26.7 σ_θ. The total volume of DSW has also increased largely (+27%, Figure 10c) at 26.8 σ_θ, which is almost entirely due to the thickening of this density layer (Figure 10b). Conversely, at 27.0 σ_θ and 27.1 σ_θ, both the fraction of DSW and the layer volume have declined, hence a decrease in DSW volume by 15% and 19%, respectively (Figure 10c).

Overall, the total volume of DSW within OSIW has slightly increased (+7%), yet changes in individual layers are considerable, and we propose that the loss of volume in the densest DSW layers is almost entirely compensated by the increased amount of lighter DSW. This compensation is consistent with the decrease in sea ice production described by Kashiwase et al. (2014). We thus theorize that with a reduction of sea ice production and brine release, the salt content and density decreases within the whole water column, leading to larger amounts of lighter DSW (26.7 σ_θ–26.8 σ_θ) and smaller amounts of the heavier DSW (e.g., 27.0 σ_θ–27.1 σ_θ) being produced.

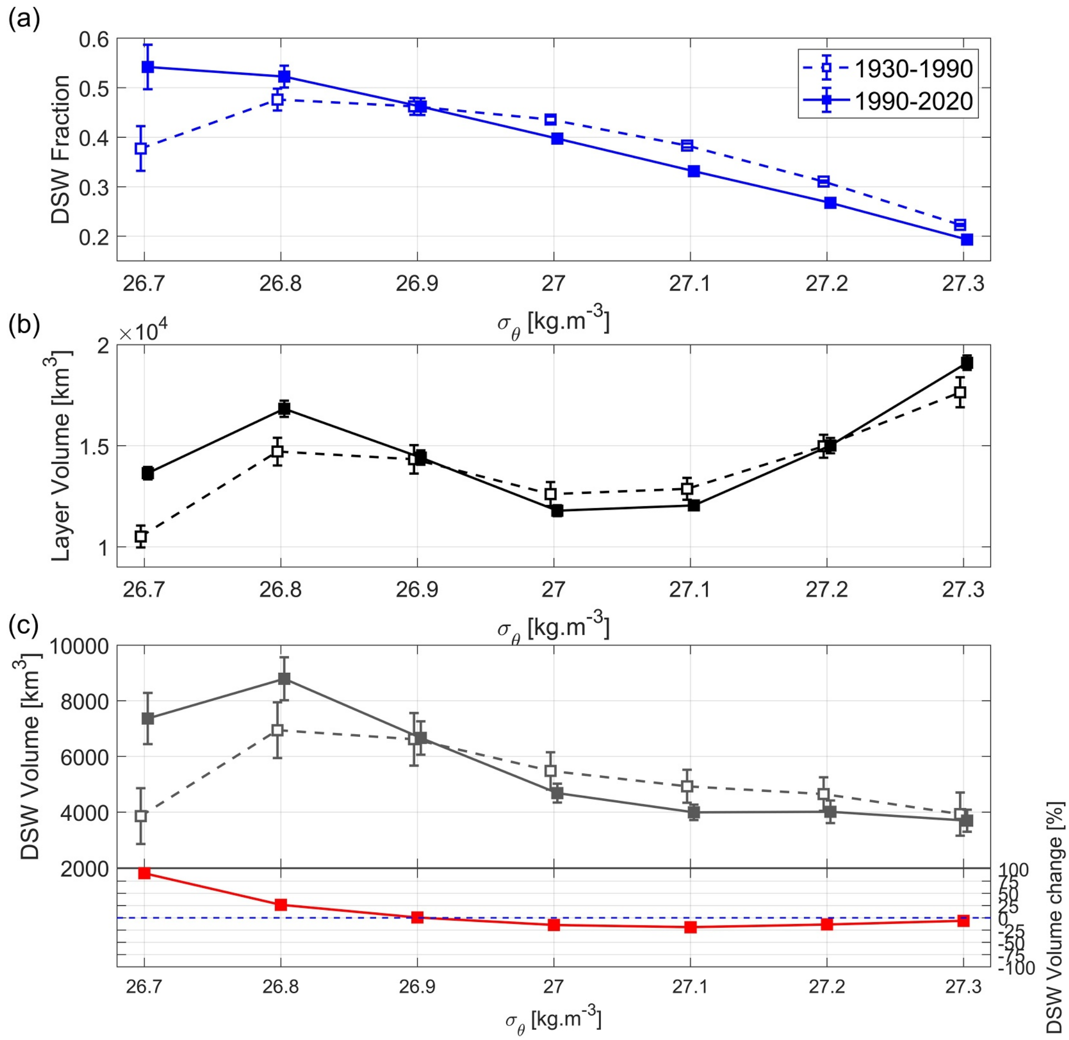

Figure 10. Yearly (a) DSW fraction, (b) isopycnal layer volume, and (c) DSW volume within the Kuril Basin for the period 1930–1990 (dashed lines) and 1990–2022 and (solid lines). The red line in the lower panel in (c) indicates the percentage changes in DSW volume. The error bars represent the 90% confidence interval.

5. Discussion

5.1. Direct Outflow of dSCW to the North Pacific

For several decades, dSCW has been considered an important source water for OSIW (Itoh et al., 2003; Watanabe & Wakatsuchi, 1998), accounting for about 5% of this water mass composition. The total volume transport of the Soya Warm Current was assumed to be directed into the Sea of Okhotsk. However, our study revealed that OSIW is made of only between 0.6% (27.0 σ_θ) and 4.5% (26.7 σ_θ) of dSCW. Averaged over the intermediate water layer between 26.8 and 27.0 σ_θ, dSCW represents only about 1% of the total composition of OSIW.

From the distribution of dSCW (Figure 5) and climatology of layer thickness for the period 1930–2022, we estimated the total volume of dSCW within the Kuril Basin to be 577 km^3. Ohshima et al. (2010) inferred a residence time of about 1 year for OSIW in the Kuril Basin and we assume a similar residence time for dSCW. Over a year, dSCW would thus enter the Kuril Basin at a rate of 0.018 Sv, which represents about 10%–20% of the total annual volume transport of dSCW flowing into the Sea of Okhotsk from the Soya Strait (0.08 Sv, Itoh et al., 2003; 0.18 Sv, Ohshima et al., 2017). Because the contribution of dSCW to OSIW is small, we suggest that dSCW also does not play a significant role in the formation of Oyashio intermediate water and NPIW.

This rough estimate of dSCW transport into the Kuril Basin implies that most of the dSCW entering the Sea of Okhotsk flows directly to the North Pacific. The exit pathway to the ocean would be through the Ekaterina Strait (sill depth ∼300 m) and Friza Strait (sill depth ∼750 m, Figure 1), as suggested by the considerably higher fraction of dSCW around the Kuril Islands (Table 2). The outflow of dSCW is expected to roughly follow the isobaths and could affect the coastal regions off eastern Hokkaido and northeastern Honshu. The existence of dSCW in these regions has not been shown yet, however. Note that the discussion above does not apply to the lighter type of dSCW (≤26.7 σ_θ), which exists within a more strongly stratified water column and whose flow is less constrained by the topography.

Chiba et al. (2021) highlighted how the use of mapped data generates artificial mixing and pseudo water masses in our study region, and erroneous estimates could also result from our climatologies. We thus calculated the dSCW fraction from raw, unmapped data following the method described in Section 2.4. These results, shown in Figures S6 and S7 of the Supporting Information S1 (Text S3) reveal a distribution of dSCW comparable to that obtained from our climatology, except for the presence of scattered points with a large (>0.2) dSCW fraction in the western and eastern part of the Kuril Basin. We acknowledge here that our mapping overlooks the effects of some processes, such as eddy shedding from the Soya Warm Current (Uchimoto et al., 2007), by which dSCW could be transported far into the Kuril Basin, hence the actual dSCW fraction in the basin could be higher. However, the general consistency between the raw and climatological distribution, the consistency of our mapped results with the distribution estimated by Chiba et al. (2021) from raw data, and the fact that most raw data in the Kuril Basin have zero dSCW fraction (Text S3 in Supporting Information S1) support our proposal that most dSCW exits through the Kuril Straits rather than contributing significantly to the formation of OSIW.

5.2. Causes of the OSIW Warming

Long-term changes in the properties of OSIW depend mainly on two factors. One is the changes in the mixing ratio of DSW and WSAW. A larger ratio of DSW would result in a colder, fresher, and more oxygenated OSIW. The other factor is the change in properties of the source water masses. If DSW properties are invariant, the changes in source water masses properties should mostly be caused by variations of the properties of WSAW. WSAW has gone through considerable warming, gain in salinity, and loss of DO (Figure 3), mainly due to a decreasing trend in the North Pacific Index (i.e., strengthening of the Aleutian Low) before 2005, which favored the transport of warm, salty, and DO-poor eastern subtropical waters into the subpolar gyre (Andreev & Baturina, 2006). The changes in WSAW properties could thus cancel the cooling, freshening, and higher-DO associated with the increased flow of DSW into the Kuril Basin at 26.7 σ_θ. To quantify the role of these two contributions on the long-term changes in OSIW properties, we apply the method by Mensah and Ohshima (2021). This method consists in calculating the properties that OSIW would have in 1990–2022 if it was made of the source waters of 1990–2022 but with the mixing ratio of the 1930–1990 period. The respective contributions of the mixing ratio and source water masses changes on the OSIW properties variations can then be inferred. The results of this experiment, estimated from yearly θ data (Figure 11a), reveal that the change in DSW fraction plays a crucial role in most layers. At 26.7 σ_θ, the increased fraction of DSW and the considerable warming of WSAW cancel each other, resulting in negligible changes in OSIW temperature and salinity. For layers of 27.0 σ_θ and denser, the change in mixing ratio is the dominant factor explaining between 60% and 99% of OSIW warming. Only at 26.8 σ_θ and 26.9 σ_θ is the change in mixing ratio small, leaving the variation of WSAW properties as the main factor explaining the warming and salinity increase in the Sea of Okhotsk. Results of the same experiment estimated from DO data (Figure 11b), support those of Figure 11a, although they are not statistically significant. At 26.7 σ_θ, the post-1990 increase in DO due to the enhanced fraction of DSW is entirely canceled by the loss of DO content of WSAW, whereas for density greater than 27.0 σ_θ, the reduced DSW fraction is the main factor explaining the lowered DO content of OSIW.

5.3. Relationship Between DSW Changes and the North Pacific Overturning

We assumed, as a basis for the theory of the weakening of the intermediate overturning, that a clear relationship exists between sea ice and DSW production (Sections 1 and 4.2). However, no such relationship has been directly observed. Figurkin's (2011) results even suggest a negative correlation between DSW density and sea ice extent, implying that a phenomenon other than sea ice production could cause changes in the DSW volume. Uehara et al.'s (2014) found that DSW (defined regardless of density) freshened between 1945 and 2005 and attributed this to the freshening of surface waters of subarctic origin, which DSW is made from. This is consistent with

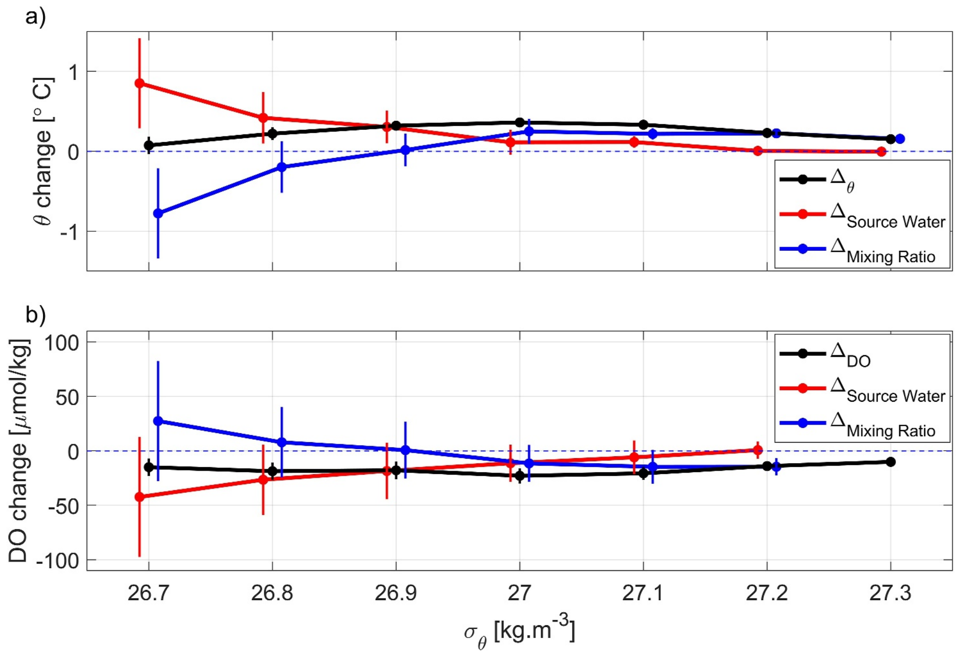

Figure 11. (a) Changes in OSIW potential temperature between the 1925–1990 and the 1990–2022 yearly climatologies (black solid line) and its contributing factors: the warming of the source waters (red solid line) and the changes in the mixing ratio between DSW and WSAW (blue line). The error bars indicate the 90% confidence interval. Panel (b) same as (a) for DO. Results of contributing factors at 27.3 σ_θ are not estimated for DO since DSW is not defined for DO at this density.

Matsuda et al.'s (2015) explanation that surface salinity anomalies originating in the subarctic gyre and the Bering Sea are conveyed to the Sea of Okhotsk. Given the relationship between the strength of the subarctic gyre, WSAW properties, and the inflow of subarctic waters to the Sea of Okhotsk (e.g., Andreev & Baturina, 2006; Andreev & Watanabe, 2002; Prants et al., 2015), DSW density could be controlled more by the strength of the Aleutian Low and subarctic gyre than by local sea ice production.

To verify the validity of our assumed relationship between sea ice and DSW production, we followed a procedure akin to that of Andreev and Baturina (2006), in which the Oyashio water salinity was reproduced from a combination of the strength of the Aleutian Low, represented by the North Pacific Index (NPI, Trenberth & Hurrell, 1994), the strength of the subpolar gyre, and the 18.6-year tidal cycle. Here, we will reproduce OSIW salinity at 27.0 σ_θ from such a model, with and without the addition of a sea ice production parameter.

First, we produced a yearly time series of OSIW salinity at 27.0 σ_θ for all years with more than 10 data points, and the time series is smoothed with a 3-year moving averaged filter. The time series runs from 1964 to 2019, as the smoothed time series is continuous in this range, and exhibits a clear increasing trend. We then constructed a modeled OSIW by using the winter (November–March) NPI, which should reflect the changes in WSAW salinity (Andreev & Baturina, 2006), the winter Sverdrup Transport (ST) between 46°N and 50°N to represent the variability of subarctic waters transport to the Sea of Okhotsk (Ohshima et al., 2010), and a sine signal to represent the 18.6-year tidal cycle (Figures 12a and 12b), as follows:

$$S_{\mathrm{OSIW}}(y) = a + b \cdot \mathrm{NPI}(y) + c \cdot \mathrm{ST}(y) + d \cdot \cos(2\pi(y - 1969 - \varphi)/18.6 \quad (3)$$

where a is an offset, b, c, and d are the amplitudes of each signal, y is year, 1969 is a reference year for the tidal cycle, and φ is the phase lag for the tidal signal. All the time series are smoothed with a 3-year moving average filter. This model represents all the non-sea ice production-related contributions to OSIW properties. A least-square fit to the salinity time series yields a correlation coefficient of 0.57 ($p < 0.01$, Figure 12c).

Further, we added a sea ice production term to this model:

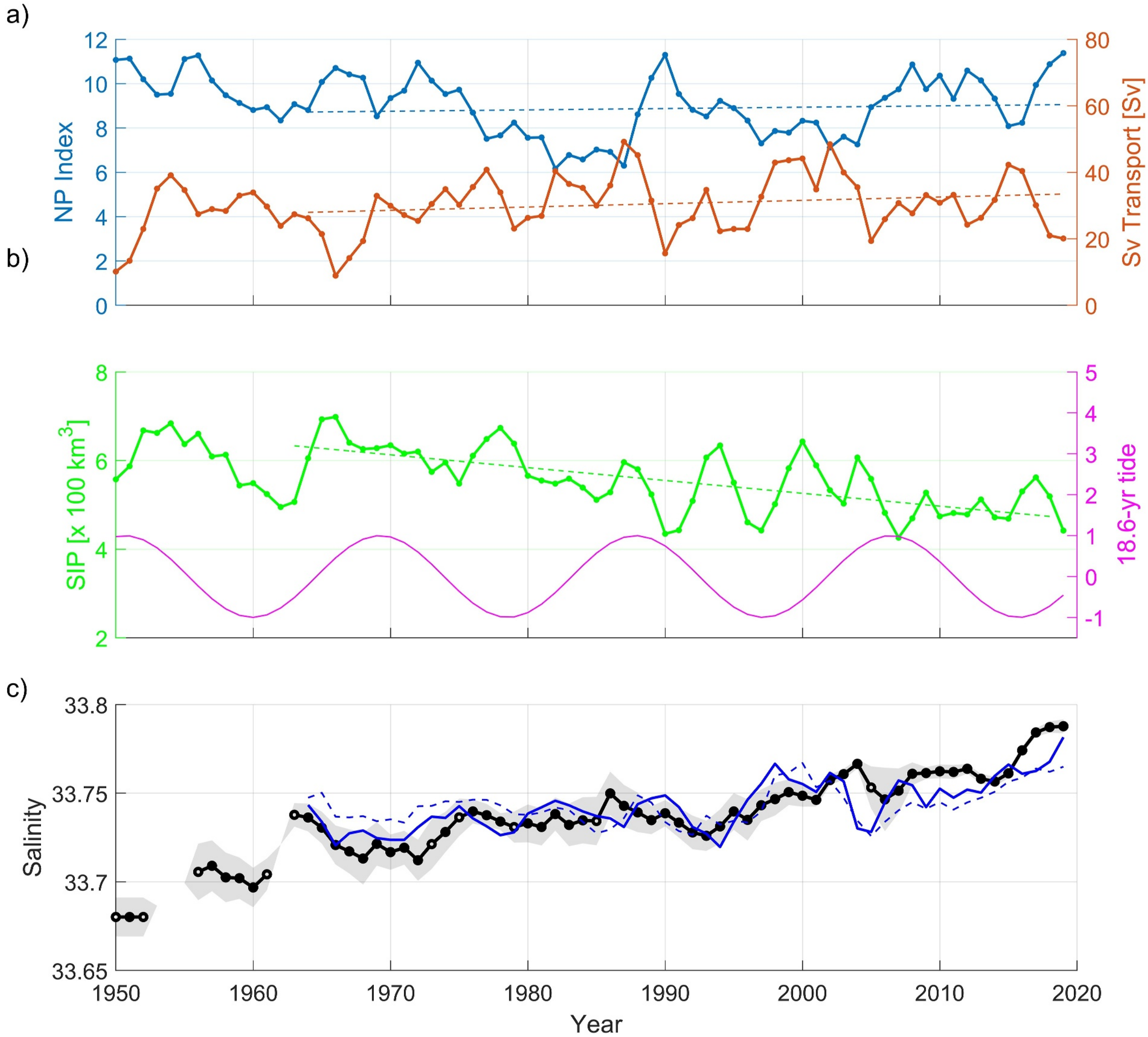

Figure 12. 3-year smoothed time series of (a) winter North Pacific Index and Sverdrup transport, (b) proxy sea ice production in the Sea of Okhotsk and 18.6-year diurnal tidal cycle, and (c) OSIW salinity at 27.0 σ_θ (black line) and fitted salinity with a model including all four parameters in (a) and (b) (solid blue line) and excluding the sea ice production (dashed blue-line). In (a) and (b) the straight dotted lines represent the trends from 1964 to 2019. In (c), the shade represents the 95% confidence interval and the empty dots represent 3-year smoothed data points in which at least 1 year of data was missing. The Sverdrup Transport in (a) was estimated from ERA5 hourly data (Hersbach et al., 2023).

$$S_{\mathrm{OSIW}}(y) = a + b \cdot \mathrm{NPI}(y) + c \cdot \mathrm{ST}(y) + d \cdot \cos\left(\frac{2\pi(y - 1969 - \varphi)}{18.6}\right) + e \cdot \mathrm{SIP}(y) \tag{4a}$$

Here, SIP is the proxy yearly sea ice production, obtained following Kashiwase et al. (2014) regression to the satellite-derived sea ice production:

$$\mathrm{SIP} = (-\,0.17 \cdot X1 - 0.15 \cdot X2 + 1.20 \cdot X3) - 3.28 \tag{4b}$$

where $X1$ is the late autumn temperature in the northwest region, $X2$ is the winter temperature in the north region, and $X3$ is the winter meridional wind speed in the north region (see Kashiwase et al., 2014 for details on the regions and averaging periods.). Here, SIP represents only the sea ice production contributed by atmospheric variables, and of the 4 parameters in Equation 4a, it is the only one which exhibits a significant trend (Figure 12b). The modeled OSIW salinity following Equation 4 fits well with OSIW salinity (Figure 12c), with a correlation coefficient of 0.77 (0.72 for the unsmoothed salinity time series, $p < 0.001$). The large increase in correlation coefficient suggests that sea ice production is an important factor controlling the properties of OSIW via the volume of DSW produced: when sea ice production is high (low), more (less) DSW is produced at the 27.0 σ_θ level and OSIW salinity decreases (increases). Equation 4a yields significant ($p < 0.01$) correlation coefficients when fitted to the salinity at any density level between 26.8 σ_θ and 27.2 σ_θ. The coefficients for Equation 4a at 27.0 σ_θ are $a = 33.715$, $b = 0.0083$, $c = 0.0011$, $d = 0.0144$, $e = -0.0137$ and $\varphi = 6.6$ years.

The results of Figure 12 thus suggest that the control of OSIW by sea ice production has a similar order of magnitude as the control by subarctic waters properties and influx (Equation 3). However, our modeled OSIW salinity in Equation 4a still does not account for the variations of the sea surface salinity (SSS), which also affect DSW salinity (Uehara et al., 2014) and density. Both the SSS in the northeastern Sea of Okhotsk and the SIP exhibit a large decreasing trend. Therefore, it is unclear to which extent the long-term variations of SSS or those SIP are responsible for the increase in OSIW salinity. We also note that the variations of SIP and those of OSIW salinity are not well related at the interannual-to-decadal scale (Figures 12b and 12c). While SIP affects the DSW density and volume by the amount of brine rejected during sea ice formation, SSS changes the initial value of salinity from which DSW is made. These two processes are practically independent from one another, and they could interact positively or negatively (i.e., canceling each other out). Such interactions might explain why the time series of SIP is not well correlated with that of OSIW salinity at time scales shorter than the trend. This might also explain why in Uehara et al. (2014), SSS in the northeastern Sea of Okhotsk and DSW salinity are uncorrelated during some periods of time. We thus suggest that both SIP and SSS could play a role in the variability OSIW properties, by changing the volume of light or heavy DSW being produced. Meanwhile, the variation in the influx and properties of WSAW is the other governing factor of the variability of OSIW properties.

The North Pacific intermediate overturning has two important components involving the Sea of Okhotsk. First is the production of sea ice which leads to the formation of DSW and its sinking to the intermediate levels. Second is the exchange of waters between the Sea of Okhotsk and the North Pacific, in which WSAW enters and OSIW exits the Sea of Okhotsk. Mensah and Ohshima (2021) demonstrated that OSIW outflowing to the North Pacific has decreased at all density layers from 26.8 σ_θ to 27.3 σ_θ, by nearly 30% in four decades. Yet, in the Sea of Okhotsk, the changes in DSW volume are not uniform in this density range. Low-density DSW has increased in volume whereas the amount of denser DSW has decreased. This implies that the relationship between DSW formation and the strength of the North Pacific intermediate overturning is not straightforward. Inside the Sea of Okhotsk, it starts with the reduction of sea ice production, which in turn leads to the lightening of DSW (possibly modulated by variations of SSS) without affecting the total DSW volume. Meanwhile, the volume of surface water entering the Sea of Okhotsk and that of intermediate waters outflowing to the North Pacific might be reduced (e.g., Mensah & Ohshima, 2021).

5.4. Implications on the Iron Availability and Biological Productivity

The high concentration of iron found in the Sea of Okhotsk is extremely important to biological productivity as this micronutrient is a limiting factor for phytoplankton growth (Kanna et al., 2014; Kishi et al., 2021; Nishioka et al., 2007). One possible source of iron could be resuspended sediment particles from the Northwestern shelf of the Sea of Okhotsk, which would be incorporated into DSW via the strong tidal mixing on this shelf (Nakatsuka et al., 2002; Nishioka et al., 2007). The high iron content of OSIW would result from the subsequent mixing of DSW into OSIW. Iron is then transported toward the North Pacific through the outflow of OSIW via the Kuril Straits (Nishioka et al., 2007, 2020). The reduction of the outflow of intermediate waters estimated by Mensah and Ohshima (2021) could thus lead to a reduction in the iron supply to the intermediate layer of the North Pacific. However, iron is also redistributed vertically via tidal mixing in the Kuril Straits (Nishioka et al., 2020), and larger amounts of iron could be available near the surface due to the increased amounts of lighter DSW (26.7–26.8 σ_θ) and the vertical mixing. In this sense, the weakening of the overturning may not necessarily induce a reduction of the iron supply to the North Pacific. Whether the reduction of OSIW outflow to the North Pacific or the increase of lighter DSW in OSIW dominates the long-term changes in iron supply to the North Pacific is an issue of crucial importance that merits further study.

6. Conclusion

In this paper, we revisited the properties of the intermediate waters in the Sea of Okhotsk and built upon previous related research works (Itoh et al., 2003; Ohshima et al., 2014; Watanabe & Wakatsuchi, 1998), taking advantage of the considerable amount of hydrographic data acquired in the Sea of Okhotsk since the year 2000, especially the addition of profiling float DO data. A new mapping technique adapted to polar and sub-polar environments (Mensah & Ohshima, 2023) also allowed us to reinterpret the water mass composition of OSIW.

One focus of this paper is the reevaluation of dSCW fraction within OSIW. The new mapping technique allowed us to map the water properties in the Sea of Okhotsk with significantly lower error than the iso-directional weighted mean mapping used in previous studies (e.g., Figure 2). The evaluation from our new climatology revealed that dSCW accounts for only 1% of OSIW, whereas a considerably higher fraction of dSCW (11%) is found in the vicinity of the southern Kuril Straits (Table 2). Our mapped distribution of dSCW (Figure 5) is consistent with that estimated from raw data by Chiba et al. (2021). We thus suggest that a large part of the dSCW entering the Sea of Okhotsk via the Soya Strait would flow along the Hokkaido coast and exit directly toward the North Pacific rather than staying in the Kuril Basin to form OSIW.

The main focus of this research is the changes in the volume of DSW within the Kuril Basin related to the multi-decadal decrease in sea ice production in the northern Sea of Okhotsk (Kashiwase et al., 2014) and the weakening of the North Pacific intermediate overturning (Itoh, 2007; Nakanowatari et al., 2007). This study follows up on the findings of Ohshima et al. (2014) who attributed the significant warming of OSIW to a decrease in DSW production. Our analysis revealed that while the overall amount of DSW in the Kuril Basin does not change significantly, the main volume of DSW is currently shifting from heavy (>26.9 σ_θ) to light waters. The total volume of DSW in the 27.0–27.3 σ_θ layer has decreased by 2,600 km^3 (Figure 10c) since 1990, which represents 14% of the volume present in the basin before this year. This change is consistent with the reduction in sea ice production and could be another expression of the weakening of the North Pacific intermediate overturning (Kashiwase et al., 2014; Mensah & Ohshima, 2021; Ohshima et al., 2014). The long-term decrease in sea surface salinity in the subarctic Pacific and the Sea of Okhotsk (Uehara et al., 2014) is also likely to play a role in the shift toward lighter DSW. We found that these changes in DSW amounts play a considerable role in the variations of OSIW properties: at the denser layers, the decrease in DSW volume explains most of the warming of OSIW whereas, at the lighter layers, the increased volume of DSW compensates totally or partially the warming (increase in salinity, loss of DO) of OSIW source waters. The differing nature of the variations in the upper and lower layers of OSIW might be reflected in the properties of NPIW, such that the salinity and temperature of the density layers above (below) NPIW's salinity minimum decreases (increases), as observed by Kouketsu et al. (2010). The role of the changes in light versus heavy DSW volume in NPIW properties is, however, still unclear. Sasano et al. (2018) described how the decreasing DO trend in the northwestern Pacific is the strongest at 26.7 σ_θ, due to a weakening of the winter convection upstream of the Oyashio. Since 26.7 σ_θ is also the layer in which the volume of DO-rich DSW has increased the most (Figure 10c), Sasano et al.'s (2018) result suggests that this increase only has a limited effect downstream of the Sea of Okhotsk. This does not apply to densities greater than 26.7 σ_θ, which are unaffected by winter convection in the North Pacific. Also, while we described the major long-term changes in OSIW properties, we note that bi-decadal variations play a smaller, but significant role in changing the properties of OSIW, the Oyashio water, and NPIW (Andreev & Baturina, 2006; Itoh, 2007; Kouketsu et al., 2010; Mensah & Ohshima, 2021; Ono et al., 2001; Osafune & Yasuda, 2006; Sasano et al., 2018).

Lastly, we suggest that the weakening of the North Pacific intermediate overturning may not necessarily induce a decrease in the iron supply to the ocean. Our rationale is that the increased amounts of DSW at the 26.7 and 26.8 σ_θ layers might enhance the quantity of iron redistributed to the surface by tidal-induced mixing in the Kuril straits.

Data Availability Statement

Historical CTD data were downloaded from the World Ocean Database 2018, a *National Centers for Environmental Information* standard product. The profiling float data in the Sea of Okhotsk from the joint University of Washington—Hokkaido University project is publicly available through the following link: http://doi.org/10.17592/001.2024052001.

Acknowledgments
This work is supported by Grants-in-Aid for Scientific Research #17H01157 and #20H05707 from the Ministry of Education, Culture, Sports, Science and Technology of Japan. We thank Y. Mitani (Kyoto University) for providing us with the biologging data from 7 instrumented seals in the Sea of Okhotsk. Data analyses were conducted using the Pan-Okhotsk Information System of Hokkaido University and all manuscript figures were drawn using MATLAB version R22b (The MathWorks, Inc. https://uk.mathworks.com/products/matlab.html). We convey our thanks to the two anonymous reviewers whose insightful and constructive comments greatly contributed to the improvement of this paper.

References

Andreev, A., & Pipko, I. (2022). Water circulation, temperature, salinity, and pCO_2 distribution in the surface layer of the East Kamchatka Current. *Journal of Marine Science and Engineering*, *10*(11), 1787. https://doi.org/10.3390/jmse10111787

Andreev, A., & Watanabe, S. (2002). Temporal changes in dissolved oxygen of the intermediate water in the subarctic North Pacific. *Geophysical Research Letters*, *29*(14), 25–31. https://doi.org/10.1029/2002gl015021

Andreev, A. G., & Baturina, V. I. (2006). Impacts of tides and atmospheric forcing variability on dissolved oxygen in the subarctic North Pacific. *Journal of Geophysical Research*, *111*(C7), C07S10. https://doi.org/10.1029/2005jc003103

Andreev, A. G., & Shevchenko, G. V. (2008). Interannual variability of water transport by the East Kamchatka and East Sakhalin Currents and their influence on dissolved oxygen concentration in the Sea of Okhotsk and subarctic Pacific. *Russian Meteorology and Hydrology*, *33*(10), 657–664. https://doi.org/10.3103/S1068373908100075

Boyer, T. P., Baranova, O. K., Coleman, C., Garcia, H. E., Grodsky, A., Locarnini, R. A., et al. (2018). NOAA atlas NESDIS 87.World Ocean Database [Dataset]. *1–207*. https://www.ncei.noaa.gov/products/world-ocean-database

Chiba, A., Horioo, I., Isoda, Y., & Kobayashi, N. (2021). Transport and alteration processes of dense Soya Current Water at the shelf-basin boundary off Abashiri. *Oceanography in Japan*, *30*(2), 15–46. https://doi.org/10.5928/kaiyou.30.2_15

Drucker, R., & Riser, S. C. (2016). In situ phase-domain calibration of oxygen Optodes on profiling floats. *Methods in Oceanography*, *17*, 296–318. https://doi.org/10.1016/j.mio.2016.09.007

Figurkin, A. L. (2011). Variability of temperature and salinity for bottom waters in the northern Okhotsk Sea. *Izvestiya Tikhookeanskogo Nauchno-Issledovatel'skogo Instituts Rybnogo Khozyalstva I Okeanografil*, *166*, 255–274.

Gladyshev, S., Martin, S., Riser, S., & Figurkin, A. (2000). Dense water production on the northern Okhotsk shelves: Comparison of ship-based spring-summer observations for 1996 and 1997 with satellite observations. *Journal of Geophysical Research*, *105*(C11), 26281–26299. https://doi.org/10.1029/1999jc000067

Gladyshev, S., Talley, L., Kantakov, G., Khen, G., & Wakatsuchi, M. (2003). Distribution, formation, and seasonal variability of Okhotsk Sea mode water. *Journal of Geophysical Research*, *108*(C6), 3186. https://doi.org/10.1029/2001JC000877

Godfrey, J. S. (1989). A Sverdrup model of the depth-integrated flow for the world ocean allowing for island circulations. *Geophysical & Astrophysical Fluid Dynamics*, *45*(1–2), 89–112. https://doi.org/10.1080/03091928908208894

Hersbach, H., Bell, B., Berrisford, P., Biavati, G., Horányi, A., Muñoz Sabater, J., et al. (2023). ERA5 hourly data on single levels from 1940 to present. *Copernicus Climate Change Service (C3S) Climate Data Store (CDS)*. https://doi.org/10.24381/cds.adbb2d47

Itoh, M. (2007). Warming of intermediate water in the Sea of Okhotsk since the 1950s. *Journal of Oceanography*, *63*(4), 637–641. https://doi.org/10.1007/s10872-007-0056-z

Itoh, M., Ohshima, K. I., & Wakatsuchi, M. (2003). Distribution and formation of Okhotsk Sea Intermediate Water: An analysis of isopycnal climatology data. *Journal of Geophysical Research*, *108*(C8), 3258. https://doi.org/10.1029/2002JC001590

Kanna, N., Toyota, T., & Nishioka, J. (2014). Iron and macro-nutrient concentrations in sea ice and their impact on the nutritional status of surface waters in the southern Okhotsk Sea. *Progress in Oceanography*, *126*, 44–57. https://doi.org/10.1016/j.pocean.2014.04.012

Kashiwase, H., Ohshima, K. I., & Nihashi, S. (2014). Long-term variation in sea ice production and its relation to intermediate water in the Sea of Okhotsk. *Progress in Oceanography*, *126*, 21–32. https://doi.org/10.1016/j.pocean.2014.05.004

Kishi, S., Ohshima, K. I., Nishioka, J., Isshiki, N., Nihashi, S., & Riser, S. C. (2021). The prominent spring bloom and its relation to sea-ice melt in the Sea of Okhotsk, revealed by profiling floats. *Geophysical Research Letters*, *48*(6), e2020GL091394. https://doi.org/10.1029/2020GL091394

Kono, T., & Kawasaki, T. (1997). Modification of the western subarctic water by exchange with the Okhotsk Sea. *Deep-Sea Research I*, *44*(4), 689–711. https://doi.org/10.1016/s0967-0637(96)00107-0

Kouketsu, S., Fukasawa, M., Sasano, D., Kumamoto, Y., Kawano, T., Uchida, H., & Doi, T. (2010). Changes in water properties around North Pacific intermediate water between the 1980s, 1990s, and 2000s. *Deep Sea Research Part II: Topical Studies in Oceanography*, *57*(13–14), 1177–1187. https://doi.org/10.1016/j.dsr2.2009.12.007

Martin, S., Drucker, R., & Yamashita, K. (1998). The production of ice and dense shelf water in the Okhotsk Sea polynyas. *Journal of Geophysical Research*, *103*(C12), 27771–27782. https://doi.org/10.1029/98jc02242

Matsuda, J., Mitsudera, H., Nakamura, T., Sasajima, Y., Hasumi, H., & Wakatsuchi, M. (2015). Overturning circulation that ventilates the intermediate layer of the Sea of Okhotsk and the North Pacific: The role of salinity advection. *Journal of Geophysical Research: Oceans*, *120*(3), 1462–1489. https://doi.org/10.1002/2014jc009995

Mensah, V., & Ohshima, K. I. (2021). Weakened overturning and tide control the properties of Oyashio Intermediate Water, a key water mass in the North Pacific. *Scientific Reports*, *11*(1), 14526. https://doi.org/10.1038/s41598-021-93901-6

Mensah, V., & Ohshima, K. I. (2023). A mapping methodology adapted to all polar and subpolar oceans with a stretching/shrinking constraint. *Journal of Atmospheric and Oceanic Technology*, *40*(10), 1241–1261. https://doi.org/10.1175/JTECH-D-22-0143.1

Mensah, V., Ohshima, K. I., Drucker, R., & Riser, S. (2024). Profiling floats data (temperature, salinity, dissolved oxygen) in the Sea of Okhotsk and the northwestern Pacific Ocean, 2002-2020., 1.00 [Dataset]. *Arctic Data archive System (ADS)*. Retrieved from https://ads.nipr.ac.jp/dataset/A20240520-001

Mensah, V., Ohshima, K. I., Nakanowatari, T., & Riser, S. (2019). Seasonal changes of water mass, circulation and dynamic response in the Kuril Basin of the Sea of Okhotsk. *Deep-Sea Research, Part A: Oceanographic Research Papers I*, *144*, 115–131. https://doi.org/10.1016/j.dsr.2019.01.012

Nakanowatari, T., Ohshima, K. I., Mensah, V., Mitani, Y., Hattori, K., Kobayashi, M., et al. (2017). Hydrographic observations by instrumented marine mammals in the Sea of Okhotsk. *Polar Science*, *13*, 56–65. https://doi.org/10.1016/j.polar.2017.06.001

Nakanowatari, T., Ohshima, K. I., & Wakatsuchi, M. (2007). Warming and oxygen decrease of intermediate water in the northwestern North Pacific, originating from the Sea of Okhotsk, 1955–2004. *Geophysical Research Letters*, *34*(4), L04602. https://doi.org/10.1029/2006gl028243

Nakata, K., & Ohshima, K. I. (2022). Mapping of active frazil and sea ice production in the Northern Hemisphere, with comparison to the Southern Hemisphere. *Journal of Geophysical Research: Oceans*, *127*(12), e2022JC018553. https://doi.org/10.1029/2022jc018553

Nakatsuka, T., Yoshikawa, C., Toda, M., Kawamura, K., & Wakatsuchi, M. (2002). An extremely turbid intermediate water in the Sea of Okhotsk: Implication for the transport of particulate organic matter in a seasonally ice-bound sea. *Geophysical Research Letters*, *29*(16), 1757. https://doi.org/10.1029/2001GL014029

Nihashi, S., Ohshima, K. I., Tamura, T., Fukamachi, Y., & Saitoh, S. (2009). Thickness and production of sea ice in the Okhotsk Sea coastal polynyas from AMSR-E. *Journal of Geophysical Research*, *114*(C10), C10025. https://doi.org/10.1029/2008JC005222

Nishioka, J., Obata, H., Ogawa, H., Ono, K., Yamashita, Y., Lee, K., et al. (2020). Subpolar marginal seas fuel the North Pacific through the intermediate water at the termination of the global ocean circulation. *Proceedings of the National Academy of Sciences of the United States of America*, *117*(23), 12665–12673. https://doi.org/10.1073/pnas.2000658117

Nishioka, J., Ono, T., Saito, H., Nakatsuka, T., Takeda, S., Yoshimura, T., et al. (2007). Iron supply to the western subarctic Pacific: Importance of iron export from the Sea of Okhotsk. *Journal of Geophysical Research*, *112*(C10), C10012. https://doi.org/10.1029/2006jc004055

Ohshima, K. I., Nakanowatari, T., Riser, S., Volkov, Y., & Wakatsuchi, M. (2014). Freshening and dense shelf water reduction in the Okhotsk Sea linked with sea ice decline. *Progress in Oceanography*, *126*, 71–79. https://doi.org/10.1016/j.pocean.2014.04.020

Ohshima, K. I., Nakanowatari, T., Riser, S., & Wakatsuchi, M. (2010). Seasonal variation in the in- and outflow of the Okhotsk Sea with the North Pacific. *Deep-Sea Research, Part II*, *57*(13–14), 1247–1256. https://doi.org/10.1016/j.dsr2.2009.12.012

Ohshima, K. I., Simizu, D., Ebuchi, N., Morishima, S., & Kashiwase, H. (2017). Volume, heat, and salt transports through the Soya Strait and their seasonal and interannual variations. *Journal of Physical Oceanography*, *47*(5), 999–1019. https://doi.org/10.1175/JPO-D-16-0210.1

Ohtani, K., Akiba, Y., & Takenouti, A. Y. (1972). Formation of western subarctic water in the Bering Sea. *Biological Oceanography of the Northern North Pacific Ocean*, 31–44.

Ono, T., Midorikawa, T., Watanabe, Y. W., Tadokoro, K., & Saino, T. (2001). Temporal increases of phosphate and apparent oxygen utilization in the surface waters of western subarctic Pacific from 1968 to 1998. *Geophysical Research Letters*, *28*(17), 3285–3288. https://doi.org/10.1029/2001gl012948

Osafune, S., & Yasuda, I. (2006). Bidecadal variability in the intermediate waters of the northwestern subarctic Pacific and the Okhotsk Sea in relation to 18.6-year period nodal tidal cycle. *Journal of Geophysical Research*, *111*(C5), C05007. https://doi.org/10.1029/2005jc003277

Prants, S. V., Andreev, A. G., Budyansky, M. V., & Uleysky, M. Y. (2015). Impact of the Alaskan Stream flow on surface water dynamics, temperature, ice extent, plankton biomass, and walleye pollock stocks in the eastern Okhotsk Sea. *Journal of Marine Systems*, *151*, 47–56. https://doi.org/10.1016/j.jmarsys.2015.07.001

Riser, S. C. (1996). Ventilation and formation of North Pacific intermediate water. In *Biogeochemical processes in the North Pacific, proceedings of the international marine science symposium* (pp. 12–20). Mutsu.

Rogachev, K. A. (2000). Recent variability in the Pacific western subarctic boundary currents and Sea of Okhotsk. *Progress in Oceanography*, *47*(2–4), 299–336. https://doi.org/10.1016/S0079-6611(00)00040-9

Sasano, D., Takatani, Y., Kosugi, N., Nakano, T., Midorikawa, T., & Ishii, M. (2018). Decline and bidecadal oscillations of dissolved oxygen in the Oyashio region and their propagation to the western North Pacific. *Global Biogeochemical Cycles*, *32*(6), 909–931. https://doi.org/10.1029/2017gb005876

Shcherbina, A. Y., Talley, L. D., & Rudnick, D. L. (2003). Direct observations of North Pacific ventilation: Brine rejection in the Okhotsk Sea. *Science*, *302*(5652), 1952–1955. https://doi.org/10.1126/science.1088692

Shu, H. W., Mitsudera, H., Yamazaki, K., Nakamura, T., Kawasaki, T., Nakanowatari, T., et al. (2021). Tidally modified western boundary current drives interbasin exchange between the Sea of Okhotsk and the North Pacific. *Scientific Reports*, *11*(1), 12037. https://doi.org/10.1038/s41598-021-91412-y

Stabeno, P. J., Reed, R. K., & Overland, J. E. (1994). Lagrangian measurements in the Kamchatka Current and Oyashio. *Journal of Oceanography*, *50*(6), 653–662. https://doi.org/10.1007/bf02270498

Takizawa, T. (1982). Characteristics of the Sôya Warm Current in the Okhotsk Sea. *Journal of the Oceanographical Society of Japan*, *38*(5), 281–292. https://doi.org/10.1007/BF02114532

Talley, L. (1993). Distribution and formation of North Pacific Intermediate Water. *Journal of Physical Oceanography*, *23*(3), 517–537. https://doi.org/10.1175/1520-0485(1993)023<0517:dafonp>2.0.co;2

Trenberth, K. E., & Hurrell, J. W. (1994). Decadal atmosphere-ocean variations in the Pacific. *Climate Dynamics*, *9*(6), 303–319. https://doi.org/10.1007/bf00204745

Uchimoto, K., Mitsudera, H., Ebuchi, N., & Miyazawa, Y. (2007). Anticyclonic eddy caused by the Soya Warm Current in an Okhotsk OGCM. *Journal of Oceanography*, *63*(3), 379–391. https://doi.org/10.1007/s10872-007-0036-3

Uehara, H., Kruts, A. A., Mitsudera, H., Nakamura, T., Volkov, Y. N., & Wakatsuchi, M. (2014). Remotely propagating salinity anomaly varies the source of North Pacific ventilation. *Progress in Oceanography*, *126*, 80–97. https://doi.org/10.1016/j.pocean.2014.04.016

Uehara, H., Kruts, A. A., Volkov, Y. N., Nakamura, T., Ono, T., & Mitsudera, H. (2012). A new climatology of the Okhotsk Sea derived from the FERHRI database. *Journal of Oceanography*, *68*(6), 869–886. https://doi.org/10.1007/s10872-012-0147-3

Watanabe, T., & Wakatsuchi, M. (1998). Formation of 26.8–26.9 σθ water in the Kuril Basin of the Sea of Okhotsk as a possible origin of North Pacific Intermediate Water. *Journal of Geophysical Research*, *103*(C2), 2849–2865. https://doi.org/10.1029/97jc02914

Yasuda, I. (1997). The origin of the North Pacific Intermediate Water. *Journal of Geophysical Research*, *102*(C1), 893–909. https://doi.org/10.1029/96jc02938

References From the Supporting Information

Uchida, H., Kawano, T., Kaneko, I., & Fukasawa, M. (2008). In situ calibration of optode-based oxygen sensors. *Journal of Atmospheric and Oceanic Technology*, *25*(12), 2271–2281. https://doi.org/10.1175/2008jtecho549.1